UNCLASSIFIED MASTER COPY FOR REPRODUCTION PURPOSES

SECURITY CLASSIFICATION OF THIS PAGE

REPORT I

1a. REPORT SECURITY CLASSIFICATION: Unclassified

AD-A230 839

2a. SECURITY CLASSIFICATION AUTHORITY

2b. DECLASSIFICATION / DOWNGRADING SCHEDULE

Approved for public release; distribution unlimited.

4. PERFORMING ORGANIZATION REPORT NUMBER(S)

5. MONITORING ORGANIZATION REPORT NUMBER(S): ARO 22966.3-MS

6a. NAME OF PERFORMING ORGANIZATION: UNIVERSITY OF ILLINOIS

6b. OFFICE SYMBOL (If applicable)

7a. NAME OF MONITORING ORGANIZATION: U. S. Army Research Office

6c. ADDRESS (City, State, and ZIP Code): URBANA IL 61801

7b. ADDRESS (City, State, and ZIP Code): P. O. Box 12211, Research Triangle Park, NC 27709-2211

8a. NAME OF FUNDING / SPONSORING ORGANIZATION: U. S. Army Research Office

8b. OFFICE SYMBOL (If applicable)

9. PROCUREMENT INSTRUMENT IDENTIFICATION NUMBER: DAAL03-86-K-0034

8c. ADDRESS (City, State, and ZIP Code): P. O. Box 12211, Research Triangle Park, NC 27709-2211

10. SOURCE OF FUNDING NUMBERS

PROGRAM ELEMENT NO.	PROJECT NO.	TASK NO.	WORK UNIT ACCESSION NO

11. TITLE (Include Security Classification): STRENGTH OF POLYMER INTERFACES

12. PERSONAL AUTHOR(S): R. P. WOOL

13a. TYPE OF REPORT	13b. TIME COVERED	14. DATE OF REPORT (Year, Month, Day)	15. PAGE COUNT
FINAL	FROM 1/86 TO 1/89	90/11/25	

16. SUPPLEMENTARY NOTATION: The view, opinions and/or findings contained in this report are those of the author(s) and should not be construed as an official Department of the Army position, policy, or decision, unless so designated by other documentation.

17. COSATI CODES		
FIELD	GROUP	SUB-GROUP

18. SUBJECT TERMS (Continue on reverse if necessary and identify by block number): POLYMER WELDING, INTERFACE STRUCTURE, FRACTURE, FATIGUE, LAMINATION, DIFFUSION, * Polymers, Polymer interfaces

19. ABSTRACT (Continue on reverse if necessary and identify by block number)

Studies of strength development at polymer-polymer interfaces are examined and applications to welding of similar and dissimilar polymers are considered. The fracture properties of the weld, namely, fracture stress, σ, fracture energy, GIc, fatigue crack propagation rate da/dN, and microscopic aspects of the deformation process are determined using compact tension, wedge cleavage, and double cantilever beam healing experiments. The mechanical properties are related to the structure of the interface via microscopic deformation mechanisms involving disentanglement and bond rupture. The time dependent structure of the welding interface is determined in terms of the molecular dynamics of the polymer chains, the chemical compatibility, and the fractal nature of diffuse interfaces. Several experimental methods are used to probe the weld structure and compare with theoretical scaling laws. Results are given for symmetric amorphous welds, incompatible and compatible asymmetric amorphous welds, incompatible semicrystalline and polymer-metal welds. The relevance of interface healing studies to thermal, friction, solvent and ultrasonic welds is discussed. (25)

20. DISTRIBUTION / AVAILABILITY OF ABSTRACT: ☒ UNCLASSIFIED/UNLIMITED ☐ SAME AS RPT. ☐ DTIC USERS

21. ABSTRACT SECURITY CLASSIFICATION: Unclassified

22a. NAME OF RESPONSIBLE INDIVIDUAL: RICHARD P. WOOL

22b. TELEPHONE (Include Area Code): (217) 333-2468

22c. OFFICE SYMBOL

DD FORM 1473, 84 MAR — 83 APR edition may be used until exhausted. All other editions are obsolete.

SECURITY CLASSIFICATION OF THIS PAGE: UNCLASSIFIED

STRENGTH OF POLYMER INTERFACES

by

Richard P. Wool

(217) 222-2468

Department of Materials Science and Engineering
University of Illinois, 1304 W. Green St., Urbana, Illinois 61801

Final Report, Proposal No. 22966-MS
Army Research Office, Durham, NC

Version 4.0

Nov., 1990

ABSTRACT

Studies of strength development at polymer-polymer interfaces are examined and applications to welding of similar and dissimilar polymers are considered. The fracture properties of the weld, namely, fracture stress, σ, fracture energy, GIc, fatigue crack propagation rate da/dN, and microscopic aspects of the deformation process are determined using compact tension, wedge cleavage, and double cantilever beam healing experiments. The mechanical properties are related to the structure of the interface via microscopic deformation mechanisms involving disentanglement and bond rupture. The time dependent structure of the welding interface is determined in terms of the molecular dynamics of the polymer chains, the chemical compatibility, and the fractal nature of diffuse interfaces. Several experimental methods are used to probe the weld structure and compare with theoretical scaling laws. Results are given for symmetric amorphous welds, incompatible and compatible asymmetric amorphous welds, incompatible semicrystalline and polymer-metal welds. The relevance of interface healing studies to thermal, friction, solvent and ultrasonic welds is discussed.

INTRODUCTION

The joining or welding of polymers can be accomplished by several techniques involving thermal welding, vibrational welding, friction welding, solvent welding, surface chemical modification, ion beam surface modification, resonance heating and other more exotic but less common techniques. In this Report we focus on polymer welding where the molecules near the surfaces become mobile and the weld strength develops by a combination of surface rearrangement, wetting and diffusion. The molecular mobility can be induced by heat from friction, (ultrasonic) vibration, impact, hot plates, solvents, etc.

In recent years, we have considered the problem of strength development at polymer-polymer interfaces in terms of the static and dynamic properties of random-coil chains (1-4). When two pieces of molten polymer are brought into contact, wetting or close molecular contact (van der Waals) first occurs followed by interdiffusion of chain segments back and forth across the wetted interface. After a contact time, t, we inquire as to the mechanical energy, G, required to separate the two pieces as a function of time, temperature, T, contact pressure, P, and molecular weight, M, of the linear random-coil chains, i.e.,

$$G = W(t, T, P, M) \tag{1}$$

where W is the welding function to be determined. Solutions to this problem have application to similar situations involving polymer-polymer interfaces. For example, processing of powder and pellet resin, internal weld lines of polymer melts during extrusion and injection molding, welding of surfaces, lamination of composites, coextrusion, and autohesion of uncured linear elastomers.

In this Report, we focus on problems of welding and autohesion with emphasis on symmetric interfaces where the same amorphous polymer exists on both sides of the interface. Consideration is also given to the important case of incompatible asymmetric amorphous and crystalline interfaces where strength develops between two immiscible polymers. We begin by introducing the reptation model (5, 6) for diffusion at a symmetric interface and determine a molecular description of the interface structure as a function of the variables, t, T, P, and M. We then discuss models to relate the interface structure to the mechanical properties via a set of microscopic deformation mechanisms. The latter involve disentanglement by chain pullout, bond rupture and connectivity between chains. The predictions for welding, tack and green strength are compared with experiments and theories (7-11) of other investigators.

THEORY

Molecular Dynamics of Random-Coil Chains

The motion of individual chains in amorphous bulk materials or concentrated solutions of linear random-coil (Gaussian) chains has been modelled by the reptation theory of de Gennes (5) and Edwards (6). In this model the chain is confined to a tube having a similar shape as the random-coil configuration of the chain. The tube represents topological constraints to lateral motion of monomers imposed by the neighboring chains via entanglements and predominantly restricts motion of the chain to that along the curvilinear length of the tube. Our use of this model is illustrated in Fig. 1. At t = 0, the chain (solid line) is in its initial tube indicated by the dashed lines. The chain exhibits Brownian motion back and forth in the tube and because the chain ends are free to move in any direction away from the tube, the memory of the initial tube position in space is gradually lost as shown at times t_2 and t_3. However, the chain being in a dense system is always in a new tube but only parts of the chain, usually towards the center, retain memory of the initial tube for the relaxation time, T_r. The length of chain, l(t), which "escapes" from the initial tube is also a random-coil chain obeying Gaussian statistics and we call it the minor chain (2). As the minor chain increases in length we can represent its static dimensions by a "most probable" spherical envelope as shown in Fig. 1.

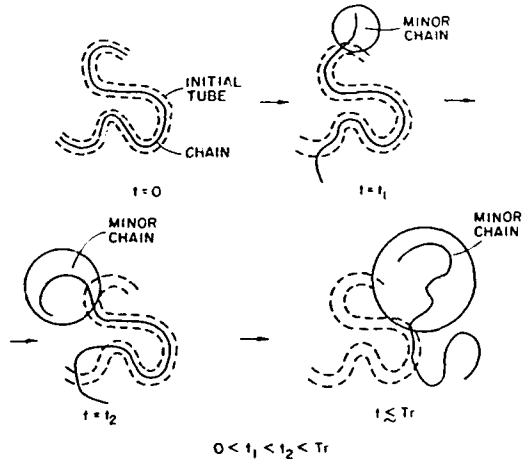

Fig. 1. The reptation model for a random-coil chain in an entangled melt shows the chain relaxing from its original configuration or tube at times $0<t_1<t_2\leq T_r$ where T_r is the tube disengagement or relaxation time. The minor chain is the portion of the chain which has relaxed from its original configuration and is shown contained in its random-coil most probable spherical envelope. The dotted tube represents the topological constraints to motion imposed by the neighboring chains in the melt (Kim and Wool).

Finally at $t = T_r$, the reptation time, the chain has escaped or forgotten its original configuration. The following relations summarize the description of the motion of a linear polymer chain in an entangled melt:

The mean square escape length of the minor chains, $\langle l^2 \rangle$:

$$\langle l^2 \rangle = 16 D_1 t/\pi. \qquad (2)$$

The curvilinear one-dimensional diffusion coefficient, D_1:

$$D_1 \approx M^{-1}. \quad (3)$$

The mean square monomer displacement of the minor chains:

$$\langle X^2 \rangle \approx \langle l^2 \rangle^{1/2}. \quad (4)$$

The mean square center-of-mass diffusion distance, $\langle X^2_{cm} \rangle$:

$$\langle X^2_{cm} \rangle \approx 2Dt. \quad (5)$$

The center-of-mass self-diffusion coefficient, D:

$$D \approx M^{-2}. \quad (6)$$

The reptation time, T_r:

$$T_r \approx M^3 \quad (7)$$

The fraction of chain remaining in the tube, F(t):

$$F(t) = 1 - 4/\pi^{3/2}(t/T_r)^{1/2}, \quad (8)$$

where $t < T_r$. For $t > T_r$, F(t) can be well approximated by (5, 12),

$$F(t) \approx 8/\pi^2 e^{-t/T_r}. \quad (9)$$

Equations 8 and 9 form the basis for describing the viscoelastic shear relaxation modulus of the Doi-Edwards(12) constitutive theory of entangled linear polymer melts. Considerable experimental support exists for the molecular weight dependence of the self-diffusion coefficient, Eq. 5, and has been reviewed by Tirrell (13). Support for the minor chain model shown in Fig. 1 has recently been obtained by Lee and Wool and by Walczak and Wool (14). Using FTIR techniques, they showed that the orientation relaxation of step-strained centrally deuteriated polystyrene chains first occurred by relaxation of the protonated chain ends while the center of the chain retained its orientation. The chains were diluted in a higher molecular weight matrix. The centrally deuteriated part of the triblock chain then relaxed at a predicted time and rate consistent with the reptation theory. The homopolymer chains (without the higher molecular weight matrix) do not show this effect which we believe is due to the percolation relaxation mechanism recently proposed by us. However, the reptation theory fails to accurately predict the molecular weight dependence of the zero-shear viscosity with a 3.4 power law exponent. The relaxation time, $T_r \approx M^3$, is also important in determining healing or welding times at polymer interfaces. In the next section we use the minor chain model to develop a time and molecular weight dependent molecular description of a polymer interface. Effects of temperature and pressure will also be discussed.

Molecular Description of a Polymer-Polymer Interface

The most important interface to consider is that formed by a symmetric A/A polymer pair consisting of linear monodisperse molecular weight polymers whose chain ends are uniformly distributed in the bulk melt material. Polydisperse symmetric A/A pairs and some asymmetric A/B pairs can also be investigated using methods presented in this section. Assuming instantaneous wetting (time-dependent wetting is considered later) of the two surfaces we proceed to analyze the molecular aspects of the interface arising from interdiffusion. This problem is simplified further using the minor chain model as shown in Fig. 2.

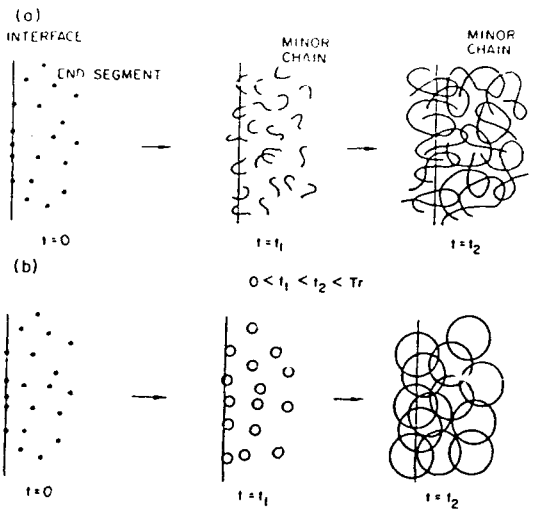

Fig. 2. The interdiffusion process at a polymer-polymer interface in terms of the behavior of (a) the minor chains and (b) the minor chain spherical envelopes. Only one side of the interface is shown for convenience. Instantaneous molecular contact or wetting is assumed at t=0 (Kim and Wool).

At t = 0, molecular contact is achieved at the interface (only the molecules on one side of the interface are shown for clarity). The chains begin to reptate via their chain ends which are shown initially as dots randomly distributed in space. As time proceeds, only that part of the chain which has escaped its original configuration, i.e., the minor chain, can contribute to interdiffusion across the interface. Furthermore, we do not have to consider the exact location of each segment of the minor chain but only the spherical envelope to which it belongs, as shown in Fig. 2. Thus, as time approaches the reptation time, T_r, interpenetration and reentanglement of chains are achieved and the molecular properties of the virgin state are obtained at the interface plane. From this minor chain model, many molecular aspects of the interdiffusion process can be determined, as presented below. Solutions are given for $t < T_r$ (healing) and $t > T_r$ (virgin state). Details of the calculations are given in references 2, 3, and 15.

Number of Chains Intersecting the Interface, n(t)

The number of random-coil chains intersecting unit area of the interface as a function of contact time, t, and molecular weight, M, behaves as,

$$n(t) \approx t^{1/4} M^{-5/4}; \quad (t < T_r) \tag{10}$$

$$n_\infty \approx M^{-1/2}. \qquad (t > T_r) \tag{11}$$

A chain is considered to intersect the interface when one of its ends has crossed the interface contact plane defined at t = 0. n(t) also scales as X/M where X is the average monomer segment interpenetration distance defined by Eq. 4. Eq. 10 is derived on the basis that all chains whose ends are within a distance of X from the interface will have intersected the interface at time t, and that the number of chains per unit volume varies as M^{-1}. The time-dependence is a typically $t^{1/4}$ rather than $t^{1/2}$ as expected for usual atomic diffusion processes.

Note that the static or virgin state solution at $t > T_r$ is obtained by substituting for the reptation time, $T_r \approx M^3$ in the dynamic solution. The static solutions are independent of the molecular dynamics model and can be derived from other considerations. Eq. 11 was derived previously by Wool and Rockhill (17). Thus, the dynamic solutions give the static solutions simply by substituting for the molecular weight dependence of the relaxation

time. This is an important feature in evaluating molecular aspects of strength development.

When a molecular property is suggested as controlling the time dependence of welding, that property can be used to simultaneously predict both the molecular weight dependence of welding and the molecular weight dependence of fracture in the virgin state. This three way concurrence is useful in evaluating potential solutions to welding problems. For example, it is known from the experiments of Kausch, et al. (18-20) and Wool, et al. (1, 21, 22) that the fracture stress during crack healing and welding increases as $\sigma \approx t^{1/4}$. It could be hypothesized upon inspection of Eq. 10 that the number of chains intersecting the interface, $n(t) \approx t^{1/4}$, is responsible for the strength development. However, this hypothesis can be rejected by examining the virgin state property, Eq. 11, since the fracture stress of polymers does not decrease with increasing molecular weight as $\sigma_\infty \approx M^{-1/2}$. Further experimental study would show that the healing rate does not depend on $M^{-5/4}$. Conversely, molecular properties used to describe the virgin state strength can also be evaluated by their ability to describe the time and molecular weight dependence of healing. This argument applies when the same microscopic deformation mechanisms are operative during welding and fracture of the virgin state.

Average Interpenetration Contour Length, l(t)

The average contour length of chain segments or cilia which have diffused across the interface is obtained from the minor chain model as,

$$l(t) \approx t^{1/2} M^{-1/2} \tag{12}$$

$$l_\infty \approx M \tag{13}$$

This property has the same scaling relation as the minor chain length, $\langle l \rangle$. It will be shown later that l(t) is important in determining mechanical properties where disentanglement and chain pullout are dominant microscopic deformation mechanisms.

Number of Bridges Crossing Interface, p(t)

Each time a piece of interdiffusing chain crosses back and forth through the interface, it creates a molecular bridge. Intuitively, this may be visualized as a "sewing up" of the interface. p(t) is determined by $p(t) = n(t)\sqrt{l(t)}$ where $\sqrt{l(t)}$ is proportional to the number of bridges created by each minor chain (a random walk of N steps originating at a plane will cross the plane $\sqrt{N}$ times). Thus we obtain,

$$p(t) \approx t^{1/2} M^{-3/2} \tag{14}$$

$$p_\infty \approx M^0. \tag{15}$$

This result was first obtained by de Gennes (9) using a scaling law and is equivalent to the "crossing density" determined by Prager and Tirrell (7) from a more detailed calculation of the interdiffusion process. Note that the virgin state number of bridges is independent of molecular weight. Thus, bridges alone cannot be used to describe strength development during welding in cases where the virgin strength exhibits a molecular weight dependence over some range of molecular weight as observed for most polymers.

Modifications to the bridge models have been suggested by Adolf Tirrell and Prager (7) and later by Mikos and Papas (29) which involve a minimum interpenetration depth, X_e, to develop entanglements. These approaches introduced a molecular weight dependence for

the virgin state, resolving the problem posed by Eq. 15 and gave a more complex expression for the time dependence of healing. Extrapolation of long time healing data to zero strength is predicted by this modification to intersect the time axis at a finite time, t_e, required to diffuse to the minimum distance X_e. This effect has not been observed in many welding studies conducted by various groups.

Polydispersity effects were also considered by Adolf, Tirrell and Prager (7). Assuming independent reptating chain diffusion, the contribution to the concentration profile from individual chains can be readily determined for any molecular weight distribution. At short times, the contribution from the faster diffusing shorter chains dominates the weld strength followed later by the slower diffusing longer chains. This can result in highly nonlinear welding behavior as demonstrated by McGarel and Wool (54) for welding of polystyrene. Bridge concepts are also useful in the development of entanglement models and for estimating the number of broken bonds in brittle fracture.

Average Monomer Interpenetration Depth, X(t)

The average monomer interpenetration depth of segments on the interdiffusing chains, X(t), is obtained from an integration over the Gaussian segment density profiles of the interdiffused minor chain population, (2) as shown in Fig. 3, such that,

$$X(t) \approx t^{1/4} M^{-1/4}; \tag{16}$$

$$X_\infty \approx M^{1/2} \approx R/\sqrt{6} \tag{17}$$

At $t=T_r$, the average monomer interpenetration distance is equal to the radius of gyration, or $X_\infty = R/\sqrt{6}$. The $t^{1/4}$ dependence in Eq. 16 is unique to the correlated motion of the chains for times less than the reptation time. This result can be understood by

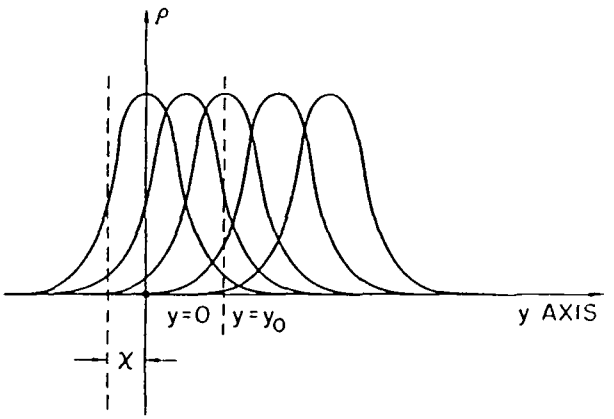

Fig. 3. Segment density, ρ, of minor chains and the average interpenetration distance, x (Kim and Wool).

considering the Brownian motion and displacement, s, of an individual monomer along the contour of the tube as $s \approx t^{1/2}$ for $t < T_r$. However, the curvilinear motion is related to translational motion via $X \approx s^{1/2}$ because the chain is a random-coil. For times greater than T_r, when the original tube has evaporated the motion of the monomer becomes uncorrelated since s is greater than the chain length and its displacement becomes similar to the center-of-mass displacement, X_{cm},

$$X_{cm} \approx t^{1/2} M^{-1} \tag{18}$$

The crossover from $t^{1/4}$ to $t^{1/2}$ behavior could be examined by experimental techniques such as Secondary Ion Mass Spectrometry (SIMS), Sputtered Neutral Atom Mass spectrometry (SNMS), (23) and Neutron Specular Reflectivity (NSR), which probe the concentration profile at a polymer interface for $t < T_r$ and distances $X < R_g$. Center of mass motion for $t > T_r$ and $X » R_g$ is well established from self-diffusion studies and found to be in agreement with Eq. 18. For chains in the bulk, the monomer motion is predicted to proceed as $t^{1/4}$ for $t < T_r$ while the center-of-mass proceeds as $t^{1/2}$ at all times. Doi and Edwards (12) showed that the center-of-mass motion is uncorrelated at all times by virtue of the random motion of the chain ends.

Eq. 18 cannot be used to describe center-of-mass motion for chains whose random-coil configurations are altered by the interface as shown in Fig. 4. The chains initially have a non-Gaussian configuration due to the reflecting boundary condition at the surface. As the minor chains interdiffuse, the configurations of the affected chains in the surface layer relax to Gaussian configurations. In Fig. 4, the average shape and size of a chain at the interface (solid vertical line) before and after relaxation are shown. The distance, η, from the location of the highest segment density of the chain to the interface remains constant during the relaxation. Since the center-of-mass of each chain is close to the peak of the segment density profile, it can be seen that very little motion of the center-of-mass occurs for $t < T_r$. For a chain in the bulk, the center-of-mass is displaced by a distance approximately equal to its end-to-end vector, R, during the same relaxation time. Since $R > \eta$, the "apparent center-of-mass self-diffusion coefficient" of chains affected by the interface would be smaller than that of chains further away from the interface in the bulk. This argument underlies the qualification for the center-of-mass scaling law in Table 1.

The nonequilibrium configurations of the chains near the interface plays an important role in determining entanglement density and the structure of asymmetric incompatible amorphous interfaces. The reduced entropy of the confined chain configurations shown in Fig. 4 acts as a driving force to achieve limited diffusion in the interface of immiscible polymers. The increase in entropy is counterbalanced by a positive enthalpy of mixing and results in an equilibrium thickness predicted by Helfand, et al. (24) as $d_\infty \approx Chi^{-1/2}$ where Chi is the Flory-Huggins interaction parameter (25).

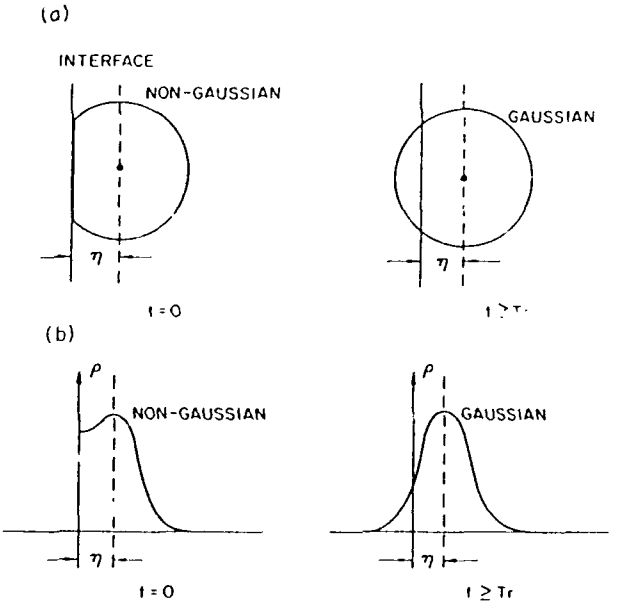

Fig. 4. (a) Average shape and size of a chain at the interface before and after healing. (b) Segment density, ρ, of the chain in (a) before and after healing (Kim and Wool).

Number of Monomers Crossing Interface, $L_o(t)$

The number of monomers which have crossed from one side of the interface to the other is equivalent to the total interpenetration contour length, $L_o(t) = n(t)l(t)$. Summing over the segment density profiles of the interdiffused minor chains, we obtain, (15)

$$L_o(t) \approx t^{3/4} M^{-7/4}; \tag{19}$$

$$L_{o\infty} \approx M^{1/2}. \tag{20}$$

The unusual $t^{3/4}$ dependence is again due to correlated motion effects and reverts to a normal $t^{1/2}$ diffusion-dependence for times greater than T_r. This result has been supported by experimental techniques discussed in reference 23 where L_o is determined from the integral of the concentration profile.

Concentration Profile

Integrating over the population of interdiffused minor chain Gaussian segment density profiles shown in Figs. 2 and 3, the normalized monomer concentration profile $\Phi(x,t)$, for the symmetric polymer-polymer interface was obtained by Zhang and Wool (15) for $t < T_r$ as,

$$\Phi(x,t) = [l(t)/L + x^2/bL]\ \mathrm{erfc}[x/(b\sqrt{2n})] \tag{21}$$

$$- \sqrt{(2n/\pi)}\ (x/L)\ \exp[-x^2/(2nb^2)]$$

where b is the bond length, n is the number of monomers in the minor chain of length l(t), x is the diffusion depth such that x = 0 at the interface and L is the contour length of the entire chain. The time dependence of the concentration profile in Eq. 21 derives from the time-dependence of the minor chains via $l(t) = \sqrt{(16\, D_1\, t/\pi)}$.

Computed concentration profiles are shown in Fig. 5 at fractional reptation times and diffusion depths normalized with respect to the end-to-end vector of the Gaussian chains (15). Fig. 5 clearly shows that the concentration at the initially joined interface at x = 0 is discontinuous when the welding time is shorter than the reptation time. For normal

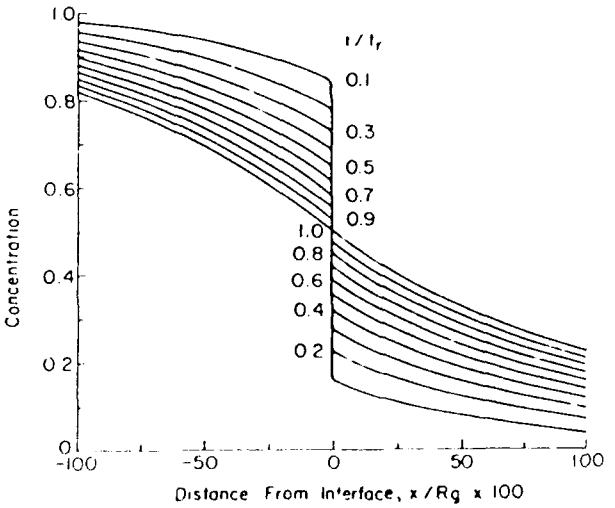

Fig. 5. Concentration profile of a polymer-polymer interface at times t less than the reptation time, T_r. The interdiffusion depth, x, is normalized with respect to the radius of gyration, R_g (Zhang and Wool).

Fickian diffusion, the atomic or monomer concentration profile at the origin immediately attains a value of 0.5, (assuming an initially sharp interface at t = 0) since the Brownian motion of the atoms is isotropic. For polymers however, the majority of monomers in contact with the initial plane exhibit anisotropic motion due to their connectivity. They are not free to interdiffuse on the time scale of monomer motion but await the diffusion of the much smaller number of minor chain ends. Thus, $\Phi(x,t)$ contains a discontinuity at $x = 0$ which is an interesting peculiarity of the reptation model and persists for at least one reptation time. The discontinuity or gap may be difficult to observe experimentally because the short range segmental motion may obscure the gap near $x = 0$ (15). However, analysis of the entire profile shape, particularly at $x \gg 0$, should give critical insight into the reptation model. This work is in progress using Neutron Reflection.

For $t > T_r$, the concentration profile returns to the classical Fickian profile,

$$\Phi(x) = \text{erfc}(x/L_d), \tag{22}$$

where L_d is the Einstein diffusion length given by $L_d = 2\sqrt{(Dt)}$. The non-Fickian characteristics of the concentration profile due to correlated motion effects in the reptation model have been discussed by de Gennes, (9) Prager and Tirrell, (28) and by Zhang and Wool (15). Eq. 21 has also been used to calculate the molecular properties of the interface and these results are summarized in Table 1 (15).

Scaling Laws for a Polymer-Polymer Interface

The molecular properties described above and others listed in Table 1 have a convenient common scaling law which relates the dynamic properties, H(t), to the static properties, H_∞, via the reduced time, t/T_r, by (4)

$$H(t) = H_\infty (t/T_r)^{r/4}; \tag{23}$$

$$H_\infty \approx M^{(3r-s)/4}, \tag{24}$$

where r, s = 1,2,3,.....

Table 1 summarizes the average dynamic and static molecular properties of a polymer-polymer interface and lists values of r and s for individual properties. This table can be used to determine other properties and evaluate suggestions and theories relating interface structure to mechanical properties. Several of these properties have also been derived by de Gennes (9, 26, 27) and by Prager and Tirrell (7, 28, 29).

Table 1. Molecular Aspects of Interdiffusion at a Polymer-Polymer Interface.

Molecular Aspect	Symbol	Dynamic Relation $H(t)$	Static Relation H_∞	r	s
General property	$H(t)$	$t^{r/4}M^{-s/4}$	$M^{(3r-s)/4}$	r	s
No. of chains	$n(t)$	$t^{1/4}M^{-5/4}$	$M^{-1/2}$	1	5
No. of bridge	$p(t)$	$t^{1/2}M^{-3/2}$	M^0	2	6
Ave. monomer depth	$X(t)$	$t^{1/4}M^{-1/4}$	$M^{1/2}$	1	1
Total monomer depth	$X_o(t)$	$t^{1/2}M^{-3/2}$	M^0	2	6
Ave. contour length	$\ell(t)$	$t^{1/2}M^{-1/2}$	M	2	2
Total contour length, no. of monomers, N	$L_o(t)$	$t^{3/4}M^{-7/4}$	$M^{1/2}$	3	7
Ave. bridge length	$\ell_o(t)$	$t^{1/4}M^{-1/4}$	$M^{1/2}$	1	1
* Center of mass depth	X_{cm}	$t^{1/2}M^{-1}$	$M^{1/2}$	2	5
Diffusion front length	N_f	$t^{1/2}M^{-3/2}$	t^0	2	6

* This equation applies to chains in the bulk and does not apply to chains whose center of mass is within a radius of gyration of the surface.

If a mechanical property such as the fracture energy, G, is controlled by one of the properties, H(t), then the time-depenence of welding is given by $G \approx t^{r/4}$ and the molecular weight dependence by $M^{-s/4}$. Considering the complexity of the fracture mechanics and deformation mechanisms, it may be an overly simplified argument to suggest that a single molecular property defined typically over a few hundred angstrom thickness of the interface is responsible for the energy dissipation and behavior of a much larger deformation zone at the crack tip. However, the scaling laws presented in Table 1 offer a convenient framework for evaluating molecular models in terms of the static and dynamic properties of the polymer chains.

FRACTAL NATURE OF A DIFFUSION FRONT

Atomic Diffusion Front

While the concentration profile due to diffusion varies smoothly with depth as shown in Fig. 5, the diffusion field when viewed in two or three dimensions has a very rough nature. Consider the two-dimensional lattice diffusion of A-atoms (Fig. 6) into B-atoms (not shown) as discussed by Sapoval, et al (30-32). The concentration profile of A-atoms is given by the Fickian result, $\Phi(x) = \text{erfc}(x/L_d)$, where $L_d = 2(Dt)^{1/2}$ is the Einstein diffusion length at time, t, with diffusion coefficient, D. The diffusion "front" (heavy line in Fig. 6) is defined by those A atoms which are connected to the diffusion source at X = 0 via other A atoms and have an empty first or second B neighbor which is itself connected to the source of B atoms. The interface with a diffusion front is seen to consist of solid regions with lakes or holes leading down to the "seashore" and unconnected islands of A atoms in the B "sea". The presence of holes and the connectedness between atoms in the interface is important in determining electrical and mechanical properties of the interface.

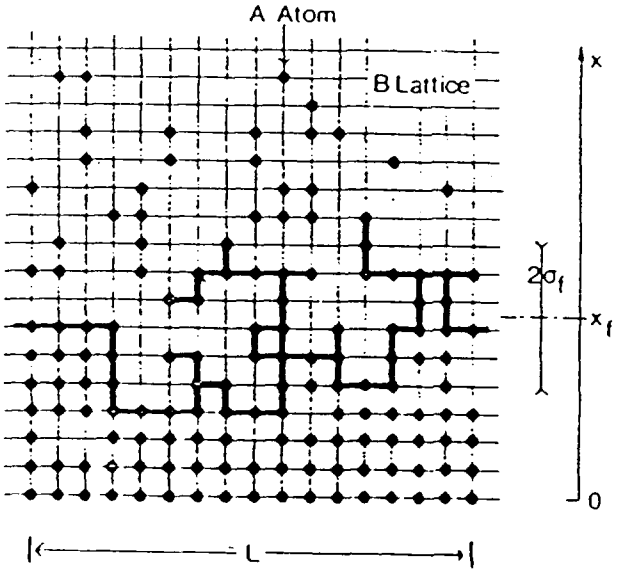

Fig. 6. Schematic of a two-dimensional diffusion field at a given time. The heavy line represents the "Diffusion Front" determined by the leading edge of A-atoms connected to their diffusion source at x = 0 and having at least one B-neighbor connected to its source. The position of the center of the front occurs at X_f and the width of the front is $2_{\sigma f}$ (From Sapoval, et al., Reference 30).

Sapoval, et al. (30-32), determined the frontier to have fractal properties involving self-similarity (scale invariance) and incompleteness of space filling (holes). The fractal geometry of the frontier is determined by the mass to radius relation, (33)

$$M \approx RD_f, \tag{25}$$

where D_f is the fractal dimension of the diffusion front. The fractal geometry exists only over the width σ_f of the front as shown in Fig. 6. In two dimensions, $D_f = 1.76$. The number of particles per unit width of the front, N_f, increases with the diffusion length according to

$$N_f = 0.96\, L_d^{\alpha}, \tag{26}$$

where the exponent α is given by,

$$\alpha = (D_f\text{-}1)\nu/(1+\nu), \tag{27}$$

in which $\nu = 4/3$ is the critical exponent for the percolation coherence length in two dimensions, resulting in $\alpha = 0.43$. The latter result is also supported by computer simulation studies of Wool and Long (34). The mean position of the frontier can be shown to occur at a concentration corresponding to the percolation threshold, p_c (30). In two dimensions, $p_c = 0.59$, such that particles in the profile at $\Phi < p_c$ are not accessible or connected while particles in the gradient at $\Phi > p_c$ are connected to the source at $x = 0$. The three-dimensional analysis of diffusion fronts is more complex (31).

Eq. 26 indicates how the interface "roughness" increases with diffusion length such that $N_f \approx L_d^{0.43}$. Thus, even though the average concentration profile varies smoothly, the diffusion front can have considerable lateral roughness as shown in Fig. 6. Experimental examples of this behavior are described in reference 34 based on studies of electrochemical reduction of metal ions diffusing in polymers by S. Mazur (35). Fig. 7 shows a polymer metal interface produced by electrochemically depositing silver atoms in a polyimide film.

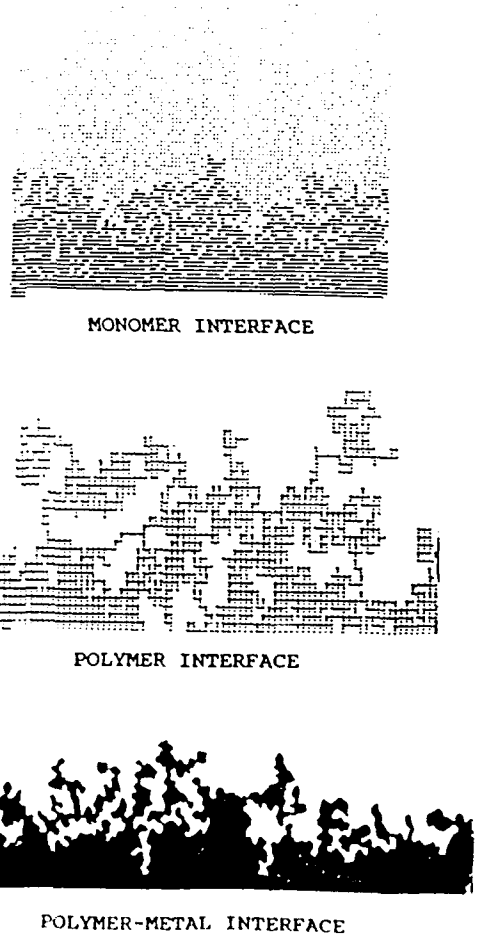

Fig. 7. Computer simulation of (a) monomer interface, (b) polymer interface, and (c) the connected region of a silver/polyimide interface (Wool and Long).

Atoms not in contact with the source (bottom of Fig. 7) were removed from the electron micrograph to reveal the highly ramified nature of the interface. The fractal dimension of the thinly sliced interface diffusion front was determined to be about 7/4 in agreement with Sapoval's theory. Details of this analysis are given in references 34 and 36.

The ability to control the interface roughness and molecular connectivity has interesting implications for the mechanical and electrical property development of interfaces. Roughness promotes mechanical interlocking but fractal characteristics with holes reduce electrical conductance and affect signal speed in the metal layer. The thickness of the conducting strip is determined by the position of the fractal diffusion front. The fractal analysis of interfaces has been found useful by us for the examination of structure development at reacting polymer-cement interfaces and for investigating biodegradation of composites containing degradable and non degradable components, e.g., starch and polyethylene blends. Biodegradation of such blends involves a percolation invasion process for materials in which the starch molecules are uniformly distributed in the PE matrix. However, when flow induced concentration profiles develop, the starch near the surface is removed by microbes while the remaining material is encapsulated within the PE matrix. The surface separating the accessed material from the encapsulated material is similar to the fractal diffusion front shown in Fig. 7.

Computer Analysis of Polymer-Polymer Interdiffusion

A computer simulation of reptating random-coil chains diffusing on a square lattice across an interface plane was conducted (34). An IBM-AT microcomputer attached to a Cray XMP-48 was used to simulate the Brownian motion of the interpenetrating chains. The object of this study was to (a) investigate the scaling laws derived for polymer interdiffusion shown in Table 1, (b) evaluate the non-Fickian concentration profiles for polymer diffusion at times less than the reptation time, and (c) to examine fractal characteristics of polymer diffusion fronts.

Brownian motion was accomplished by an algorithm which randomly chose a chain end and added a new monomer in one of three possible new directions and subtracted a monomer from the other end. The process was then repeated for each chain. The chain end distribution function was chosen to be uniform behind the interface plane. The basic reptation dynamic results were checked for consistency; namely, that (1) the relaxation time behaved as $T_r \approx M3$, (2) the center-of-mass diffusion coefficient behaved as $D \approx M-2$, and (3) that the monomer displacement r(t) behaved as,

$$\{<r(t) - r(0)>^2\}n \approx t1/2. \qquad (t<T_r) \tag{29}$$

and

$$\{<r(t) - r(0)>^2\}n \approx t \qquad (t>T_r) \tag{30}$$

where r(t) is the position vector of the nth monomer at time t. The monomer displacement average is determined over all monomers on each chain.

The chain density was chosen to be inversely proportional to the molecular weight and the monomer density in the virgin state was chosen to consist of an average of five monomers per lattice site to account for interpenetration of random-coil chain statistical segments.

At t = 0, the reptating chains were allowed to diffuse across the interface plane and formed ramified structures as shown in Fig. 7. The polymer interface is seen to consist of features resembling lakes, islands and seashore similar to the previous atomic diffusion

case. However, many of the holes near the x = 0 plane are not due to the fractal nature of diffusion but rather are due to the monomer correlated motion effect producing discontinuities in the interface as shown in Fig. 5. The computer simulation gave further support to the scaling laws shown in Table 1 and the concentration profile proposed by Zhang and Wool, Eq. 21. Fractal properties of polymer interfaces are discussed in the next section.

Fractal Polymer Diffusion Fronts

The analysis of the fractal nature of polymer diffusion fronts (34) is complicated by the interpenetrated nature of the random-coil chains allowing several statistical segments or monomers to occupy a single lattice site. Fig. 7 shows a typical ramified diffusion field for the simulated interface. The diffusion front was obtained using the same technique employed by Sapoval, et al (30). The front is potentially more ramified initially due to the connectivity of monomers within a given chain. Fig. 8 shows the number of monomer on the diffusion front, Nm, as a function of the average interdiffusion distance, <X>, for random-coil chains of molecular weights ranging from 60 to 100 statistical units. Two regions of behavior are observed.

For $t < T_r$, the front is discontinuous for reasons discussed above and Nm can be approximated by summing average contributions from single chains $\sqrt{l}(t)$ as,

$$N_m \approx n(t)\sqrt{l}(t), \tag{31}$$

where n(t) is the number of chains crossing unit area (or unit length) of the initial interface plane. From Table 1, it can be seen that n(t) scales as $n(t) \approx X(t)/M$ where X(t) is the average monomer diffusion distance (equivalent to <X> used in Fig. 8). The contribution to the diffusion front from a single minor chain is given by the square root of the contour length which is proportional to X(t). Substituting in Eq. 31 we obtain,

$$N_m \approx X(t)^2/M. \qquad (t < T_r) \tag{32}$$

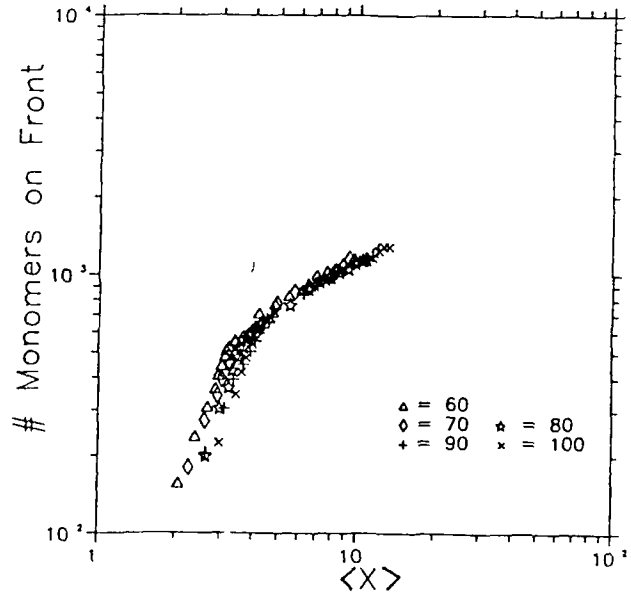

Fig. 8. The number of monomers on a polymer interface diffusion front is plotted vs. the average monomer interpenetration depth, <x>, for molecular lengths ranging from 60 to 100 times the critical entanglement length. The reptation algorithm was used to simulate Brownian motion of linear flexible chains (Wool and Long).

Fig. 8 shows that the plot of log N_m vs. log X(t) has a slope of 2 for all molecular weights and that at constant X(t), N_m varies approximately as the inverse of M. However, for times less than the reptation time, the diffusion front is not considered to be fractal since the criterion of self-similarity is not obeyed due to discontinuities in the interface plane. This concept may need to be modified when consideration is given to short range segmental motion proposed by Zhang and Wool (15). Rouse-like motion of short chain segments was not considered in this simulation and the results reflect the concentration profile for monomers on the primitive path of the reptating chain. The time-dependent scaling law for N_m at $t < T_r$ is seen from Table 1 to be identical to that for bridges, p(t).

At $t = T_r$, since $X_\infty 2 \approx M$, $N_m(T_r)$ from Eq. 32 becomes independent of molecular weight. When $t > T_r$, the number of monomers on the diffusion front is predicted from Sapoval's theory to behave as,

$$N_m \approx X^{0.43}, \tag{33}$$

and is shown by the convergence to a slope of 0.43 for all molecular weights in Fig. 8. The number of lattice sites, N_L, on the polymer diffusion front was found to behave similarly to the number of monomers, N_m. A mass-to-radius analysis of the diffusion front geometry gave a fractal dimension of approximately 1.7. These results are in agreement with the atomic diffusion fractal analysis in 2 dimensions. Thus, the diffusion front for polymers becomes fractal at times greater than the reptation time and at diffusion distances greater than the end-to-end vector of the chains.

MICROSTRUCTURAL FRACTURE CRITERIA

Chain Pullout

The Griffith approach to brittle fracture is given by (37)

$$(\delta U/\delta a)_\delta \geq 2\Gamma, \tag{34}$$

where U is the stored strain energy consumed at constant displacement, δ, to advance a crack by the increment, δa, and create surface energy, $2\Gamma\delta a$. The fracture energy, or the critical strain energy release rate, G_{Ic}, is related to Γ by

$$G_{Ic} = 2\Gamma. \tag{35}$$

In principle, if one independently knows the surface energy, Γ, of a solid one should be able to predict its fracture energy using Eq. 35. However, for high molecular weight entangled polymers the experimental values are typically of the order $G_{Ic} \approx 1000$ J/m^2 and $\Gamma \approx 10^{-2}$ J/m^2. Closer agreement with the Griffith theory is obtained for brittle fracture of very low molecular weight unentangled polymers (38, 39).

The Griffith idea has considerable value if one can determine how stored energy is consumed in forming the fracture surface. To address welding and healing problems a stored strain energy approach to fracture was adopted which considers both chain pullout via disentanglement and chain fracture mechanisms at the interface. Consider a volume element containing a small area of interface as shown in Fig. 9 subjected to normal stresses, σ_{ij}, and shear stresses, τ_{ij}. The strain energy density, U, of the element is given by,

$$U = (\sigma^2_{xx} + \sigma^2_{yy} + \sigma^2_{zz})/2E$$

$$- (\sigma_{xx}\sigma_{yy} + \sigma_{yy}\sigma_{zz} + \sigma_{xx}\sigma_{zz})_{\nu}/E \qquad (36)$$

$$+ (\tau^2_{xy} + \tau^2_{xz} + \tau^2_{yz})/2\mu_S,$$

where E, ν and μ_S are Young's modulus, Poisson's ratio and shear modulus, respectively.

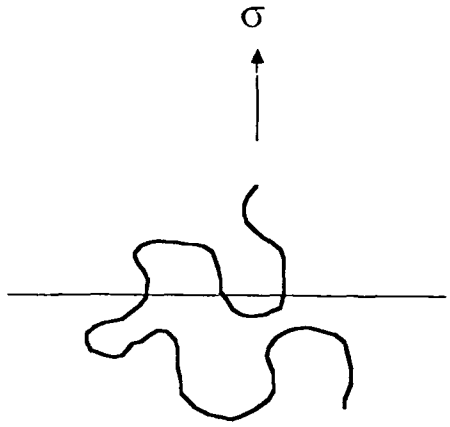

Fig. 9. A segment of a stressed chain at an interface is shown.

We first consider a uniaxial stress field with $\sigma = \sigma_{xx}$ and all other stress terms equal to zero. In that case, the strain energy density is

$$U = \sigma^2/2E. \qquad (37)$$

We can reasonably assume that the modulus behaves as, (1, 40)

$$E \approx t^O M^O; \qquad (38)$$

$$E_\infty \approx M^O, \qquad (39)$$

such that E can be assumed to remain constant during healing and fracture.

The number of chains per unit volume, N_v, is

$$N_v = o\, N_a/M, \qquad (40)$$

where o is density and N_a is Avogadro's number. The strain energy per chain, U_c, is therefore obtained as,

$$U_c = U/N_v = \sigma^2 M/(2E\, o\, N_a). \qquad (41)$$

The strain energy associated with a segment of chain of length l, is similarly derived as

$$U_c \approx \sigma^2 l. \qquad (42)$$

The stored elastic energy can be used to either pull the chain out from the interface or fracture the chain. A fracture criterion for chain pullout can be written as

$$U_c \geq Up \qquad (43)$$

where U_p is the energy to pull a chain out of its tube with a force f, and velocity, dl/dt.

The pullout force is given by $f = \mu\, dl/dt$, where μ is the friction coefficient for the chain segment of length, l. The friction coefficient for the segment is related to the monomer friction coefficient, μo, via $\mu = \mu o l$ such that the force may be written as,

$$f = \mu_o\, l\, dl/dt. \tag{44}$$

The energy required to pull a segment out at constant velocity is determined from

$$U_p = \mu_o \int_{l=0}^{l=L} l(dl/dt)\, dl, \tag{45}$$

as, (41)

$$U_p = \mu_o\, (dl/dt)\, l^2/2, \tag{46}$$

or

$$U_p \approx l^2.$$

A similar result is obtained if the chain is pulled out at constant force rather than at constant velocity, $V = dl/dt$. Eq. 46 has also been derived by Prentice (42) and Evans (43).

Substituting Eqs. 42 and 46 in Eq. 43, the critical fracture stress for chain disentanglement (and tack) is obtained as,

$$\sigma \approx (\mu_o V E b\, o\, N_a/M_o)^{1/2}\, l(t)^{1/2}, \tag{47}$$

or,

$$\sigma \approx X(t), \tag{48}$$

such that

$$\sigma \approx \sqrt{l(t)}$$

where $X(t) \sim \sqrt{l(t)}$ is the average monomer segment interpenetration distance, M_o is the monomer molecular weight, and b is the bond length. Examining the scaling laws in Table 1, the fracture stress or tack in uniaxial tension should behave as,

$$\sigma \approx t^{1/4}\, M^{-1/4}, \tag{49}$$

and the virgin (green) strength as

$$\sigma_\infty \approx M^{1/2}. \tag{50}$$

The velocity dependence, V = dl/dt, of tack and green strength during peel adhesion tests from Eq. 47 should behave as,

$$\sigma \approx V^{1/2}. \tag{51}$$

Fracture by the chain pullout mechanism is favored at low molecular weight (small l(t)), low deformation rates (small V), high temperature (low μ_o), short healing times (small l(t)) and plasticizing agents (low μ_o).

Fracture Mechanics of Welding

The Dugdale model (44) was used as a first approximation to determine the molecular aspects of the fracture mechanics. In this model, shown in Fig. 10, a crack of initial length ao propagates through a plastic line zone or craze of length rp, ahead of the crack tip. The

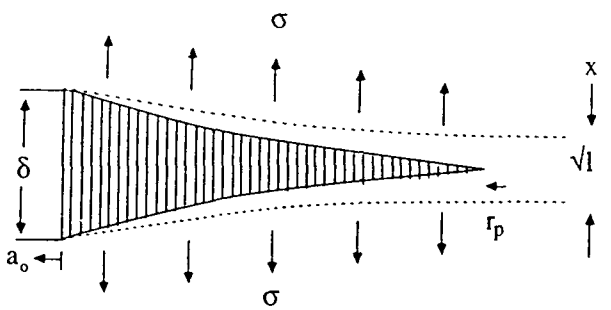

Fig. 10. The Dugdale model for a crack propagating through a welded interface of thickness X -$l^{1/2}$ is shown. The stress, σ, acting on the plastic zone of length r_p, draws the interface into craze-like fibrils of constant draw ratio, \, which break down to produce the crack opening displacement, δ (R. P. Wool).

plane stress field near the crack for a Cartesian volume element, xyz, and angle α at distance r is given by Rice (45) as,

$$\sigma_{xx} = K_I/\sqrt{2\pi r} \cos \alpha/2 \,(1-\sin \alpha/2 \sin 3\alpha/2) + \ldots\ldots ;$$

$$\sigma_{yy} = K_I/\sqrt{2\pi r} \cos \alpha/2 \,(1+\sin \alpha/2 \sin 3\alpha/2) + \ldots\ldots ; \tag{52}$$

$$\sigma_{xy} = K_I/\sqrt{2\pi r} \cos \alpha/2 + \ldots\ldots ,$$

where K_I is the stress intensity factor. The length of the plastic zone is determined by

$$r_p = \pi/8 \, K_{Ic}^2/\sigma^2_c, \tag{53}$$

where σ_c is the craze or yield stress.

The critical crack opening displacement is given by

$$\delta = K_{Ic}^2/\sigma_c \, E, \tag{54}$$

where E is the tensile modulus.

Using the approximation that σ_c remains constant within the plastic zone, the critical strain energy release rate, G_{Ic}, is determined by

$$G_{Ic} = \sigma_c \delta, \tag{55}$$

such that the fracture energy is determined as a critical force acting over a critical distance.

Fig. 11 shows the essential features of the Dugdale model for a crack propagating through a line deformation zone in styrene-isoprene-styrene (SIS) block copolymer (46). The microstructure elucidated by Transmission Electron Microscopy (TEM) consists of styrene spheres (white) with a diameter of ca 250 Å in an isoprene matrix (stained black with osmium tetroxide). For the craze zone, $r_p \approx 3\ \mu m$ and $\delta \approx 0.2\ \mu m$. The craze propagates in the stress field applied normal to the craze by incorporating a single styrene sphere into the tip of the zone. As the zone propagates it thickens from 250 Å to 2,000 Å by drawing further material into the zone and elongates by extending the material already in the zone. At the crack tip, many styrene spheres have been drawn into the zone and deformed nonuniformly such that the crack tends to propagate through the center of the zone. Similar mechanisms have been identified for crazes propagating through pure amorphous polystyrene (47, 48). Thus, a critical stress nucleates the line zone at distance r_p from the crack tip and the crack opening displacement is determined by the breakdown of the material drawn into the zone.

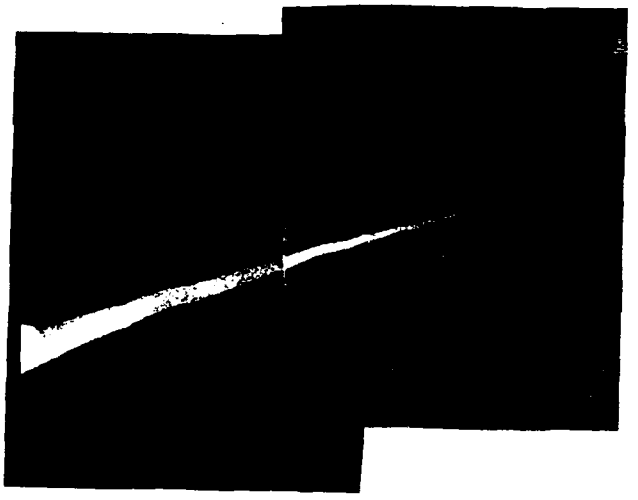

a

b

Fig. 11. (a) Transmission Electron micrograph of a plastic zone, $r_p = 3\ \mu m$, in a mechanically stressed Styrene-Isoprene-Styrene thin film. The white spheres (styrene) have a diameter of ~250 Å. The number of spheres in the zone increases towards the crack tip ($\delta = 0.2\ \mu m$) due to zone thickening. (b) Shows details at a crack tip, $\delta = 1.0\ \mu m$, and plastic deformation zone extending into the undeformed S-I-S sample. (Dolman, Robertson and Wool).

To evaluate the molecular aspects of the welding problem we first calculate σ_c using the strain energy approach such that the stored energy per molecule in an xy-plane stress field is,

$$U_c = (\sigma^2_{xx}/2E + \sigma^2_{yy}/2E + \sigma^2_{xy}/2\mu)/N_v. \quad (56)$$

Substituting for the stress terms from Eq. 52 in Eq. 56, U_c is found to be dominated by the σ_{yy} term and can be well approximated by

$$U_c \approx \sigma^2_{yy}\, l(t), \quad (57)$$

where l(t) is again the average interpenetration length. Using the same criterion for chain pullout, Eq. 46, and letting $\sigma_{yy} = \sigma_c$ at critical conditions, then

$$\sigma_c \approx l(t)^{1/2}, \quad (58)$$

which is similar to the result obtained for the uniaxial case. For glassy polymers, σc can be related to the craze stress which differs from the shear yielding stress, σ_y.

The critical crack opening displacement, δ, is determined by the breakdown of the entanglement network in the deformation zone and the extent to which the zone can thicken as depicted in Fig. 10. During welding, the zone consists of interdiffused short chain segments mixed with longer chains with nonequilibrium configurations and the entangled structure is complex. The crack opening displacement consists of two components: a component from the virgin material, δ_v, and a component from the the diffuse interface, δ_i, such that $\delta = \delta_v + \delta_i$. At low welding strengths the contribution from the weaker interface dominates since the energy required to thicken and propagate the zone into the virgin material is too high. The crack opening displacement is then determined by the breakdown of the entanglement network in the interface by the following approximation (50),

$$\delta \approx \alpha_f l(t)^{1/2}, \quad (59)$$

where α_f is the constant uniaxial draw ratio to tighten the slack between entanglements.

At this point we briefly consider an entanglement model which can be used to visualize the breakdown process of the deformation zone at the crack tip shown in Fig. 10. An entangled amorphous linear chain network is shown schematically in Fig. 12. The bridge theory of connectivity in an amorphous network proposed by Wool (3, 4) requires that the number of bridges p, crossing any load bearing plane exceeds the number of chains n, intersecting the plane. In terms of a single chain argument, this implies that each chain must be long enough to create one link or bridge, i.e., the chain minimally forms one circle or knot with its surroundings as shown in Fig. 12. The critical entanglement molecular weight M_c, occurs at p = n and is given by (3, 4)

$$M_c = 30.89(zb/c)^2 M_0\, C_\infty j \quad (60)$$

in which z,b,c,M_0, C_∞ and j are the number of monomers per c-axis length (see examples below), the bond length, the c-axis length, the monomer molecular weight, the characteristic ratio and the number of bonds per monomer, respectively. For example, with

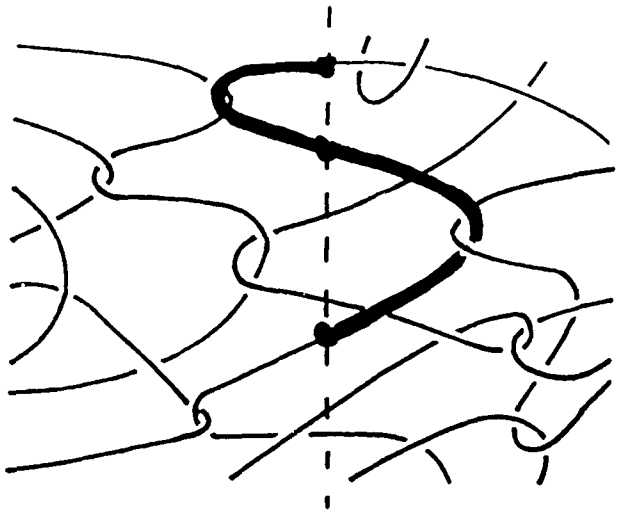

Fig. 12. An entangled network of linear polymer chains is shown. The bold structure illustrates the minimum bridge structure required of each chain to form the network.

polystyrene, b = 1.54 Å, c = 6.5 Å for an isotactic chain, z = 3 monomers per helical repeat distance, M_0 = 104, C_∞ = 10, j = 2 c-c bonds per monomer, such that Eq. 60 predicts Mc = 32,000. This compares well with the critical entanglement molecular weight for the cross-over of the zero shear melt viscosity from Rouse ($\eta \approx M$) to entangled behavior ($\eta \approx M^{3.4}$). For polyethylene, b = 1.54 Å, c = 2.55 Å, z = 1, M_0 = 28, C_∞ = 6.7, and j = 2 such that M_c = 4,000. The calculated values compare well with experiment and can be approximated for most vinyl polymers by $M_c \approx 30\, C_\infty\, M_0$.

Applying this model to examine disentanglement as a function of draw ratio, α, the number of chains crossing any plane normal to the applied strain increases as $n(\alpha) = \alpha n_\infty$ and the number of bridges increases more slowly as $p(\alpha) = p_\infty \alpha/(\alpha^2 + 1/\alpha)^{1/2}$. At the critical point of $p(\alpha) = n(\alpha)$, the critical draw ratio is determined by $\alpha_c^2 + 1/\alpha_c = 2M/M_c$ such that,

$$\alpha_c = (8/3\ M/M_c)^{1/2} \cos\{1/3 \cos^{-1} [-1/2(3M_c/2M)^{3/2}]\} \qquad (61)$$

A useful approximate solution to Eq. 61 at $M \gg M_c$ gives the critical draw ratio for disentanglement as

$$\alpha_c \approx (2M/M_c)^{1/2} \qquad (62)$$

In a welding interface, the interdiffused contour length provides new entanglements which decrease with draw ratio such that a critically connected state exists at,

$$\alpha_c \approx (2l(t)/L_c)^{1/2} \qquad (63)$$

where L_c is the entanglement contour length corresponding to M_c.

Entanglement models (49, 50) predict that the strain hardening fibril draw ratio is constant with values of $\alpha_f \approx 4$ which is in agreement with TEM studies of craze fibrils by Donald and Kramer (49). When $\alpha_c < \alpha_f$, Rouse-like retraction of the stretched entanglements will relax the contour length such that the critically connected state predicted by Eq. 63 exists. An instability arises which results in the completion of the fracture process. Substituting for σ and δ, the critical strain energy release rate is determined by

$$G_{Ic} \approx t^{1/2} M^{-1/2}; \quad (64)$$

$$G_{\infty} \approx M. \ (M < M^*) \quad (65)$$

The critical stress intensity factor, K_{Ic}, is related to the fracture energy via

$$G_{Ic} = K_{Ic}^2/E, \quad (66)$$

and is expected to increase with welding time as

$$K_{Ic} \approx t^{1/4} M^{-1/4}; \quad (67)$$

$$K_{Ic\infty} \approx M^{1/2}. \quad (68)$$

If the chains in the deformation zone cannot disentangle completely and bond rupture occurs then the scaling laws become more complicated. For welding of glassy polymers, fracture involves a mixture of disentanglement and bond rupture mechanisms. de Gennes (26) has suggested that molecular bridges could control the strength, which is similar to the crossing density suggested by Prager and Tirrell, (7) and which is similar to the total number of entanglements per chain per unit area suggested by Kausch (52). In that case, the fracture energy is given as

$$G_{Ic} \approx t^{1/2} M^{-3/2}; \quad (69)$$

$$G_{Ic\infty} \approx M^0. \quad (70)$$

The above relations for welding and fracture will be explored in the experimental section.

Stages of Healing

Healing of polymer interfaces has been described by Wool and O'Connor in terms of several stages involving (1), (a) surface rearrangement, (b) surface approach, (c) wetting, (d) diffusion and (e) randomization. Most of the above discussion focussed on the influence of diffusion on mechanical properties. However, several other factors can affect the welding process and are discussed below as the "stages of healing".

(a) Before the surfaces are contacted, one should consider the roughness or topography of the surface and how it changes with time, temperature, and pressure following contact. In fractured polymers, rearrangement of fibrillar morphology, etc., can affect the rate of crack healing. Chain end distributions near the surface can change as molecules diffuse back into the bulk polymer. Spatial changes of the molecular weight distribution may also occur, e.g., where the low molecular weight species preferentially migrate to the surface. Chemical reactions, e.g., oxidation and crosslinking can occur on the surface and complicate the molecular dynamics of diffusion. Many other processes, e.g., molecular orientation changes, can contribute to the stage of surface rearrangement. Each material and experimental technique usually possesses unique surface rearrangement processes which may need to be quantified. O'Connor (57) found significant effects of surface rearrangement on the healing rate of lightly cross-linked polybutadiene such that the fracture energy at constant healing time decreased with increasing surface

rearrangement time (prior to contact). This effect can be explained by the chain ends diffusing back into the bulk such that they were not as readily available for diffusion during healing. Recent SIMS analysis by McGarel and Wool (unpublished) of low molecular weight deuterated polystyrene chains on the surface of high molecular weight polystyrene support this concept. They found that the low molecular weight species will not preferentially migrate to the surface but will distribute uniformly in the bulk material.

(b) Surface approach considers time-dependent contact of the different parts of the surfaces to create the interface. For example, in crack, (1, 18) craze, (53, 54) and void (55, 56) healing, contact may be achieved at different locations at different times in the interface depending on the closure mode (1). For example, slow closure of a double cantilever beam crack would result in different extents of healing along the closed crack. This stage typically contributes as a boundary value problem to the other stages of wetting and diffusion.

(c) Wetting can occur in a time-dependent fashion at the interface. For our purposes we provide a brief phenomenological description of wetting to illustrate potential problems in evaluating the time-dependence of welding. Fig. 12 shows a schematic region of the plane of contact of a polymer interface (1). Due to surface roughness, etc., good contact and wetting are not achieved instantaneously at all locations. Typically, wetted "pools" are nucleated at random locations at the interface and propagate radially until coalescence and complete wetting are obtained. This problem has been treated phenomenologically as a two-dimensional nucleation and growth process such that the fractional wetted area, $\Phi(t)$, is given as (1),

$$\Phi(t) = 1 - \exp(-kt^m) \tag{71}$$

where k and m are constants depending on the nucleation function and radial spreading rates.

Contact theories proposed by Anand (72) and others suggest that complete strength may be obtained when the interface has wetted at $\Phi = 1$. Others argue that interdiffusion is necessary for strength development. The time dependence of viscous flow to promote contact and that of interdiffusion may be comparable since they are subject to the same molecular dynamic processes. We will demonstrate in later sections using both tack experiments and incompatible interface weld strength data that diffusion plays a very important role.

(d) The diffusion stage has been discussed above with respect to the instantaneous wetting condition. However, in the presence of a time dependent wetting function, Eq. 71, we see from Fig. 13 that diffusion will have progressed to different extents in different areas of the interface. If the intrinsic diffusion function, H(t) as given by Eq. 23, does not change its nature with time due to the other stages, then the net diffusion, H'(t) can be expressed as the convolution product,

$$H'(t) = \int_{-\infty}^{\tau} (t-\tau)\, d\Phi(\tau)/d\tau \; d\tau, \tag{72}$$

where τ is a "dummy" variable on the time axis. The convolution process for typical $\Phi(t)$ functions may mask the time-dependence of the intrinsic diffusion function and related

mechanical properties. This part of the problem can be solved mathematically by letting the wetting function be a Dirac delta function,

$$\frac{d\,\Phi(t)}{dt} = \delta(\tau), \tag{73}$$

such that Eq. 72 reduces to $H'(t) = H(t)$. This can be attempted experimentally by obtaining instantaneous wetting of atomically smooth surfaces under moderate contact pressure at temperatures above T_g. However, we have found that the wetting problem can result in difficulty with the analysis of most short time welding data.

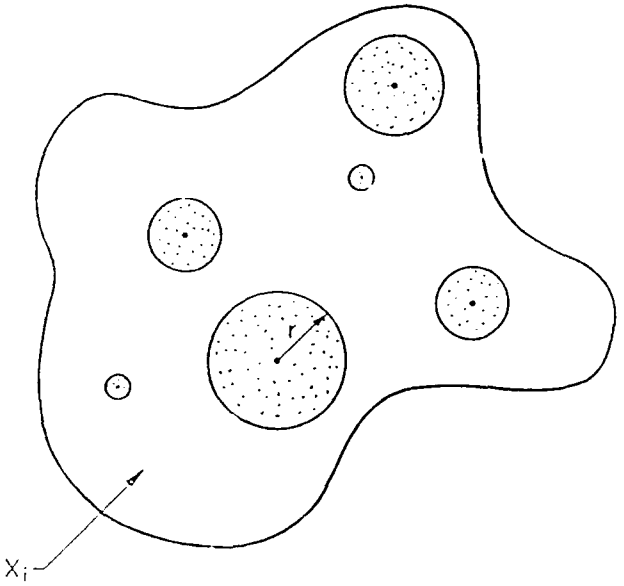

Fig. 13. A schematic view of the stages of healing in an interface. Contacted regions of radius r grow and coalesce. Interdiffusion occurs only in the wetted regions while surface rearrangement occurs in the non-wetted areas. (Wool and O'Connor)

(e) The randomization stage refers to the equilibriation of the nonequilibrium conformations of the chains near the surfaces and in the case of crack healing and processing, the restoration of the molecular weight distribution and random orientation of chain segments near the interface. The conformational relaxation is of particular importance in the strength development at incompatible interfaces.

The stages of crack healing can have interactive time-dependent functions such that the welding and tack problems can consist of processes involving five-way interconvoluted functions resulting in mechanical properties whose time dependence may not be readily interpretable. Thus, great care must be taken in conducting welding experiments which are designed to critically explore molecular theories of strength development.

HEALING EXPERIMENTS

Tack and Green Strength

The critical experiment is to show that the tack or stress at fracture of uncured linear elastomers behaves as $\sigma \approx t^{1/4}M^{-1/4}V^{1/2}$ and that the green or virgin strength behaves as $\sigma_\infty \approx (MV)^{1/2}$. In addition, the self-diffusion coefficient should be measurable as $D = A/M^2$ where A is a constant derivable from mechanical data. The concurrence of

predictions derives from the molecular dynamics analysis of tack and green strength. These predictions apply to all amorphous linear polymers whose chain configurations can be described by Gaussian statistics and whose fracture behavior is dominated by chain disentanglement mechanisms.

Fig. 14 shows tack data obtained by Skewis (61) for several polymer-polymer pairs where we have replotted the tack (units of force applied to a cross-sectional area of 0.4 cm^2) vs. $t^{1/4}$. The original data were nonlinear when plotted on a $t^{1/2}$ scale to investigate diffusion mechanisms. However, the fracture energy behaves as $G_{Ic} \approx t^{1/2}$ while the tack behaves as $\sigma \approx t^{1/4}$ as evidenced by the linear plot in Fig. 14. The SBR/Butyl pair are incompatible and the long time equilibrium strength is considerably weaker than either of the symmetric pairs. Similar $t^{1/4}$ results for tack have been reported by Wool and O'Connor (1, 40) for polybutadiene, and by Voyutskii (11) for polyisobutylene.

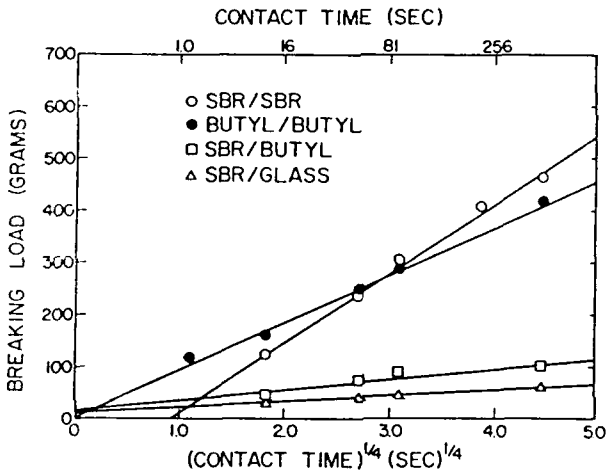

Fig. 14. The tack or breaking load vs. $t^{1/4}$ for several polymer-polymer uncured pairs as investigated by Skewis (61). Tack measurements were done with a contact load of 1000 g and a contact area of 0.40 cm^2. The viscosity-average molecular weight, M_v, of the SBR was 260,000 and 225,000 for the butyl rubber.

The molecular weight dependence of tack and green strength was investigated by Forbes and McLeod (62) for fractionated samples of Hevea. Their results are shown in Fig. 15 in which the upperline represents the green strength and the bottom line represents the tack stress evaluated at a constant contact time of t_c = 30 sec for each molecular weight. The green strength curve was obtained theoretically using (1)

$$\sigma_\infty = k_1(M^{1/2} - M_i^{1/2}), \tag{74}$$

where k_1 = 993 Pa/$M^{1/2}$ and $M_i^{1/2}$ = 284.1 is the intercept on the σ_∞ = 0 axis of the plot of σ_∞ vs. $M^{1/2}$. The curve through the tack data in Fig. 14 was determined by theory as

$$\sigma = \sigma_0 + \alpha M^{-1/4}, \tag{75}$$

where α = 5.29 MPa $M^{1/4}$ and $\sigma_0 = 80.5 \times 10^3$ Pa is a constant dependent on the initial wetting conditions of the interface. When $\sigma = k_2 t^{1/4}$ as in Fig. 14, the constant, k_2, is related to the constant, α, in Eq. 75 by

$$k_2 = \alpha/(M^{1/4}\, t_c^{1/4}), \tag{76}$$

where in this case t_c = 30 sec. Considering the difficulties in performing such experiments, the agreement between theory and experiment in Fig. 15 is satisfactory. If the strength is controlled by bridges, then $\sigma \approx M^{-3/4}$ at constant t_c and $\sigma_\infty \approx M^0$. These predictions are inconsistent with the data in Fig. 15. It has been suggested that the tack stress is independent of molecular weight but in fact it behaves approximately as $M^{-1/4}$ in close agreement with disentanglement theories. This is a weak molecular weight dependence but related mechanical properties such as fracture work, G_{Ic}, should behave with a stronger molecular weight dependence, as $G_{Ic} \approx t^{1/2}M^{-1/2}$.

In Fig. 15 the green strength is seen to rise steadily up to $M \approx 1.5 \times 10^6$ at which point it remains fairly constant and bond rupture is expected to dominate the fracture mechanism by regulating the extent of disentanglement. Given sufficient time, the tack stress will increase to the green strength value by continued diffusion. Using tracer diffusion methods, Skewis (63) measured the self-diffusion coefficient of natural rubber at 25°C as $D = 3\times10^{-14}$ cm²/sec using samples with a viscosity-average molecular weight of M_v = 234,000. The polydispersity of his samples was not known. The self-diffusion coefficient from healing data is given by (1-3)

$$D = (k_2/k_1)^4 b^2 C_\infty/6MM_0, \tag{77}$$

where C_∞ is the characteristic ratio for the dimensions of a random-coil chain. Letting M = 234,000, M_0 = 68 for polyisoprene, b = 4.05 Å from the c-axis of the cis-1,4-polyisoprene unit cell, and k_2 = 0.103 MPa/sec$^{1/4}$ from Eq. 76, we obtain $D \approx 10^{-14}$ cm²/sec which is of the same order of magnitude as $D = 3 \times 10^{-14}$ cm²/sec obtained by Skewis.

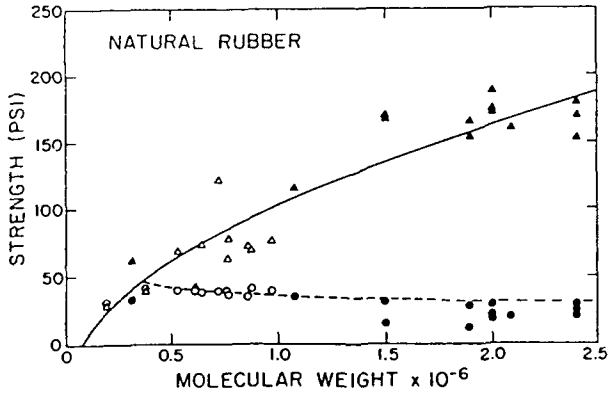

Fig. 15. Tack (circles) and green strength (triangles) as a function of viscosity average molecular weight for fractionated samples of natural rubber (Forbes and McLeod) (62). The solid line for green strength was theoretically obtained using Eq. 72 and the dashed line for tack using Eq. 73. The green strength was evaluated at a uniaxial test speed of 26.67 cm/min at 25°C, and the tack was evaluated at a constant contact time of 30 sec for each sample. Filled and unfilled data points refer to unmillled and milled natural rubber, respectively.

The reptation time, T_r, is obtained from the self-diffusion coefficient as

$$T_r = R^2/(3\pi^2 D), \tag{78}$$

where R^2 is the end-to-end vector given by $R^2 = Mj/M_0\, C_\infty\, b^2$. For natural rubber the healing time is approximated by

$$T_r = 2.48 \times 10^{-15} M^3 \text{ sec.} \quad (79)$$

When M = 234,000, T_r = 32 sec and in Fig. 15, this material should be in the green state at t_c = 30 sec as observed. The healing time required for the samples with M = 1,000,000 is about 40 min. These results differ with those of Roland and Bohm (69) who found that the time required to achieve maximum autohesive strength of polybutadiene was orders of magnitude longer than the time required for the chains to diffuse a distance approximately equal to the end-to-end vector, R. Chain branching and nonuniform wetting at the interface may have contributed to this difference.

Stacer and Schreuder-Stacer (95) investigated the time dependence of autohesion in polyisobutylene. Molecular weights of their samples ranged from 1.5-21 x 10^5 with polydispersities of 1.1 to 3.6. T-peel test configurations were used to evaluate the peel energy, G, as a function of time, molecular weight, temperature and pressure. Fig. 16 shows a plot of log G vs log t/a_T for PIB with M_w = 1.5 x 10^5. The contact time was reduced with respect to the time-temperature shift factor, a_T, to create a master plot from data obtained

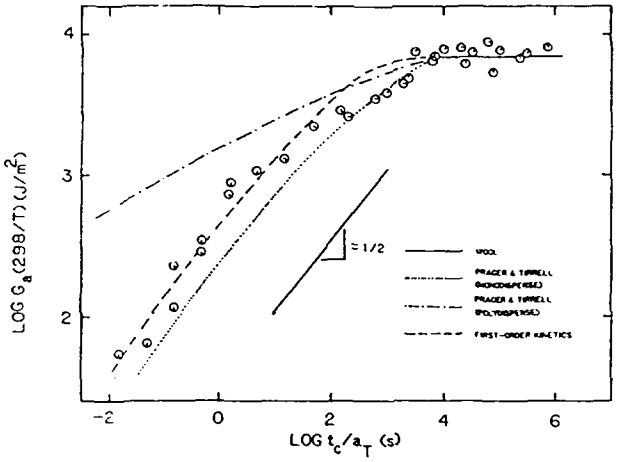

Fig. 16. Comparison of the predictions of several theoretical models with autohesion data for PIB (Stacer and Schreuder-Stacer).

at different temperatures. Several theories were examined. The scaling law for peel energy is $G \approx (t/M)^{1/2}$ as given by Wool, et al., in Eq. 64, predicts a slope of 1/2 as shown in Fig. 16. They conclude that the 1/2 power law slope is applicable to describe limited regions of the data but does not provide an overall description of the autohesion curve. The time to achieve equilibrium strength (healing time) t_∞, was predicted by Wool (3) as,

$$t_\infty = C_\infty b^2 M^3 / (6AM_0) \quad (80)$$

where A is the constant in the self diffusion coefficient relation, $D = A/M^2$. This relation was found to be in excellent agreement with the PIB autohesion data. The molecular weight dependence of healing was not properly analyzed in this work since the $M^{-1/2}$ dependence of the healing rate was incorrectly compared to the green strength energy, G_∞.

The monodisperse and polydisperse chain interdiffusion theories of Prager and Tirrell are compared with experiment in Fig. 16. This model determines the number of effective crossings per unit area where an effective crossing involves a minimum interpenetration distance related to the entanglement molecular weight spacing which allows a chain segment to participate in energy dissipative processes. The agreement is good for the monodisperse case and the polydisperse model reasonably described similar studies. Both models predict a slower rate of healing (about 1/2 time decade) compared to experiment.

Fig. 16 also compares a wetting theory of Korenevskaya, et al. (96), expressed as a first order kinetic process in terms of the fractional peel energy $G = G(t)/G_\infty$ as

$$G + \ln (1-G) = - P t/\mu$$

where P is the applied pressure and μ is the zero-shear viscosity. This relation provided excellent agreement with the data. Deviations to significantly lower G_{Ic} values were observed at short times with the high molecular weight PIB samples.

Since the diffusion controlled healing times are comparable to characteristic relaxation times of viscosity, this work cannot readily distinguish between wetting and diffusion theories. Studies by Wool and O'Connor (21, 57) of tack and healing in hydroxy terminated polybutadiene (HTPB) indicated that the mechanical property recovery due to wetting occurred in a few minutes and was a small fraction of G_∞, while interdiffusion of the partially cross-linked chains took several weeks during which the majority of the fracture energy was recovered. The separation of the relaxation times for wetting and diffusion in that case support the diffusion model.

A more convincing case for the diffusion model is obtained from studies of incompatible amorphous polymer interfaces such as PS/PMMA. At long contact times, complete wetting or contact has been achieved but the incompatibility only allows limited interdiffusion with with correspondingly low fracture energy. The observed fracture energies of incompatible interfaces by the Urbana group are consistent with the diffusion model such that the fracture energy increases as the compatibility of the polymer pairs and interdiffusion increases at constant contact area. A possible flaw in this argument is that the incompatibility influences chemical interactions, e.g., acid-base, at the contact plane which would affect the wetting theory. However, the contact plane no longer exists as such due to the limited diffusion which has occurred.

Pressure affects diffusion by decreasing the free volume which slows the hopping process necessary to achieve Brownian motion and subsequently decreases the self-diffusion coefficient. This effect is more pronounced near the glass transition temperature and is important in polymer melt processing where large hydrostatic pressures can be encountered. It is not very important in normal tack experiments where the contact pressures are usually much less than a kilobar. However, pressure affects the wetting stage by promoting better contact. Thus, tack measurements should be dependent on pressure to some degree while wetting is occurring but should be largely independent of pressure when interdiffusion is occurring. Expressions for the pressure dependence of T_r and D have been given (1, 3).

The effect of strain rate and peeling velocity on tack has been examined by many investigators. Fig. 17 shows data obtained by Hamed (64) for the cohesive strength of an SBR elastomer (FRS-146)as a function of peel rate using a T-peel test configuration. The prediction that $\sigma \approx V^{1/2}$ is observed to be in agreement with the high temperature data (where chain pullout is expected to dominate) as judged by the slope of 1/2 for the plot of log σ vs. log rate. As the temperature approaches T_g, -50°C, chain fracture begins to contribute to the deformation mechanism and the $V^{1/2}$ behavior is lost as predicted. The prediction that $\sigma \approx V^{1/2}$ is also supported by data of Tsuji, et al. (65) for T-peel tests of polyisobutylene and by data of Bhowmick, et al. (66), for adhesive tack and green strength of EPDM rubber. The dependence of the fracture energy, G, on the rate of peel is also $G \approx V^{1/2}$ since the extent of disentanglement and not the rate determines the crack opening displacement for the chain pullout mechanism.

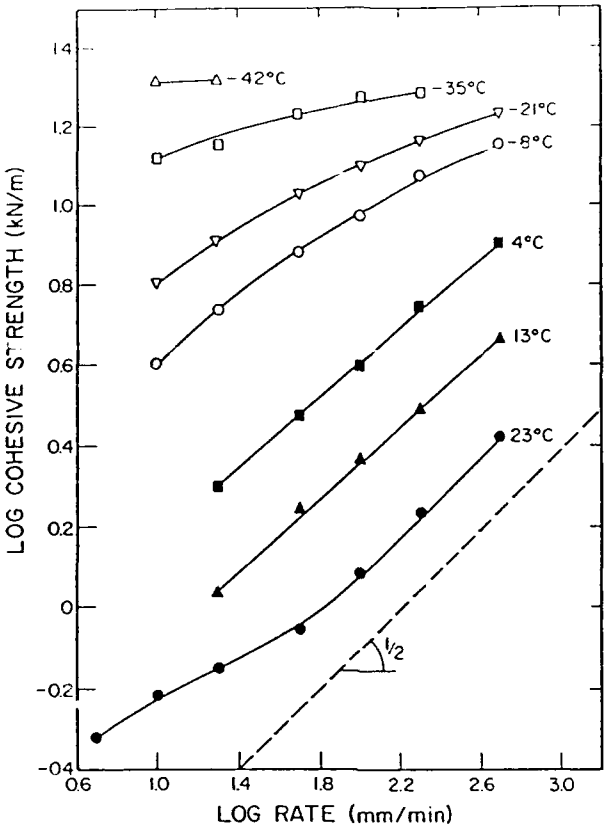

Fig. 17. Cohesive tear strength of SBR as a function of peeling rate at several constant temperatures (Hamed and Shieh) (64). The dashed line represents the theoretical slope of 1/2 and was added for comparison purposes. The SBR was a cold emulsion styrene-butadiene random copolymer containing 23% bound styrene and had a Mooney viscosity (ML-4, 100°C) of 40.

For peel adhesion, the pullout mechanism predicts the fracture energy to behave as

$$G \approx (t\,V/M)^{1/2}; \tag{81}$$

$$G_\infty \approx MV^{1/2}. \tag{82}$$

Several other theories of tack and adhesion have been presented. Bister, et al. (67), predict that the peel energy behaves as

$$G \approx M^{2/3}\,(Dt)^{1/2}. \tag{83}$$

Since $D \approx M^{-2}$ and $T_r \approx M^3$, then Eq. 82 predicts that $G \approx t^{1/2}\,M^{-5/3}$ and $G_\infty \approx M^{-1/6}$. However, this molecular weight dependence cannot be supported by data reported here or elsewhere. Most theories predict the $t^{1/2}$ dependence but as seen from Table 1, this is not a unique function.

Wu, et al. (68) predict that the adhesive strength is determined by $G \approx n(t)X(t)$ which behaves in an identical manner to bridges (Table 1) as $G \approx t^{1/2}\,M^{-3/2}$ and $G_\infty \approx M^0$. The molecular weight dependence of these relations is not supported by experiments. However, Wu, et al., also suggest that the number of chains, n(t), saturates quickly and that G depends on center-of-mass motion over larger distances as $G \approx t^{1/2}\,M^{-1}$. We disagree with the latter suggestion since n(t) increases simultaneously with the strength for times $t < T_r$.

Vasenins (70) kinetic theory of adhesion suggests that the tack stress behaves as

$$\sigma \approx t^{1/4} M^{-5/3} V.$$

While the time-dependence is supported by experiment the molecular weight and rate dependence are at variance with the body of data. Many other theories of tack and adhesion are discussed in references 10 and 71. Kausch also presents a review of crack healing studies in reference 18.

Summary of Tack and Green Strength

Strength development at a polymer-polymer interface was analyzed in terms of the dynamic and static properties of random-coil chains. Interdiffusion of chain segments across the interface was considered to be the controlling factor for tack and green strength of uncured linear elastomers. This concept is similar to that proposed by Voyutskii but differs markedly from contact theories as proposed by Anand (72) and others. In our approach, time-dependent wetting first occurs followed by interdiffusion. Increasing contact pressure and temperature should promote the establishment of molecular contact (wetting) at the interface up to a saturation point of complete wetting. However, interdiffusion is retarded by increased hydrostatic pressure and enhanced by temperature in the usual thermally activated manner. The effect of pressure on diffusion is to reduce the volume available (depending on the compressibility) for segmental motion and subsequently decrease the diffusion coefficient.

Increasing the tack test temperature increases the average interdiffusion chain segment length, as $l(T) \approx \exp -Q/2kT$, but decreases the stress required to pull the segment out, as $\sigma \approx \exp Q/4kT$, where Q is the activation energy. Therefore, the tack evaluated at constant contact time will decrease with increasing temperature for the interdiffusion controlled process.

The effect of molecular weight on tack at constant contact time, t_c, is to increase the tack according to $\sigma \approx M^{1/2}$ for those samples whose relaxation time $T_r < t_c$, and decrease the tack as $\sigma \approx M^{-1/4}$ for those molecular weights for which $T_r > t_c$. The tack should reach a maximum at a molecular weight corresponding to $T_r = t_c$. The latter value can be used to determine the self-diffusion coefficient of the chains (1). At small contact times the results might be complicated by wetting processes. The position of the maximum in a plot of σ vs. M is relatively insensitive to the contact time since $T_r \approx M^3$ and M at the maximum will consequently increase as $t_c^{1/3}$. These predictions appear to be in agreement with much experimental data reviewed by Hamed (58) and Rhee (59) but differ in some respects from their own interpretations of the same data.

The above results are not unique to elastomers and many of the predictions will be seen to describe welding and fracture of glassy polymers in the next section.

WELDING OF POLYMER INTERFACES

Symmetric Amorphous Interfaces

Fig. 18 shows the welding method used to evaluate healing relations for polymer interfaces (73, 74). Monodisperse molecular weight films (or other materials) are bonded to substrates, usually composed of the same polydisperse molecular weight material, and the film surfaces are then welded together. The film surfaces to be contacted are first molded against highly polished metal plates and annealed in vacuum to assure maximum

smoothness. To approximate the instantaneous wetting condition necessary to evaluate the effect of diffusion on welding, the surfaces are wetted at a higher temperature for a short time, $t \ll T_r$, and subsequently healed for long times at a constant lower temperature. Under these conditions, the long time healing data extrapolates to zero time.

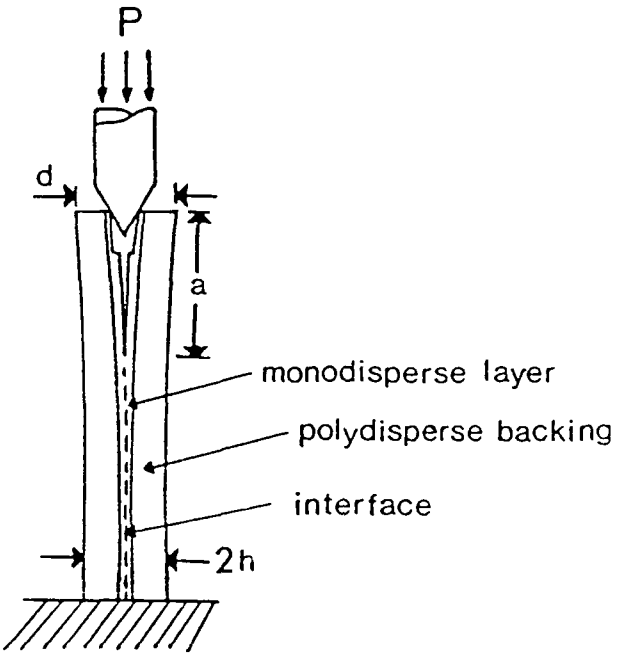

Fig. 18. Wedge cleavage method of testing strength vs. welding time in polymers. Monodisperse molecular weight films are attached to polymer substrates prior to thermal welding (Wool and O'Connor).

The stress distribution and the fracture mechanics of the wedge cleavage method have been examined (75, 76). The wedge is driven into the interface spreading the arms apart until the crack of length a begins to grow at a critical value of d as shown in Fig. 18. By modelling the specimen as an elastic double cantilever beam with each beam partly supported by an elastic foundation, the critical stress intensity factor, K_{Ic}, is obtained at constant displacement as (75, 76)

$$K_{Ic} = 3/4\ Eh3/2(d-2h)\ f(h/a)/a^2.Q, \tag{84}$$

where h is the half-width of the specimen (see Fig. 18) and d is the separation of the specimen at the upper end. The function f(h/a) is given by

$$f(h/a) = \frac{(1+0.64\ h/a)}{1 + 1.92h/a + 1.22(h/a)^2 + 0.39(h/a)^3} \tag{85}$$

and the factor Q is a correction for the extra compliance due to the presence of the end-slot (76), $Q = 1 + [(h/h')^3 - 1]\ (l_s/a)^3$, where ls is the length and h' is the half-width of the slot, respectively. The fracture energy is obtained from Eq. 84 via the relation $G_{Ic} = KIc^2/E$. The advantage of the wedge cleavage technique is that the crack propagates in a stable manner such that multiple data points can be obtained from a single sample thus providing good statistics. It is possible to obtain the weld strength as a function of welding

time by alternating crack propagation with healing treatments such that each measurement corresponds to crack advance into a previously unfractured portion of the interface.

Fig. 19 shows results obtained by O'Connor and Wool (corrected for initial wetting) for welding monodisperse molecular weight polystyrene interfaces at 120°C. The best fit to the data gives,

$$K_{Ic} \approx t^{1/4} M^{-x}, \tag{86}$$

where x is in the range 0.31 to 0.37. The latter value can be compared to the chain pullout prediction of x = 0.25 and the bridge fracture prediction of x = 0.75.

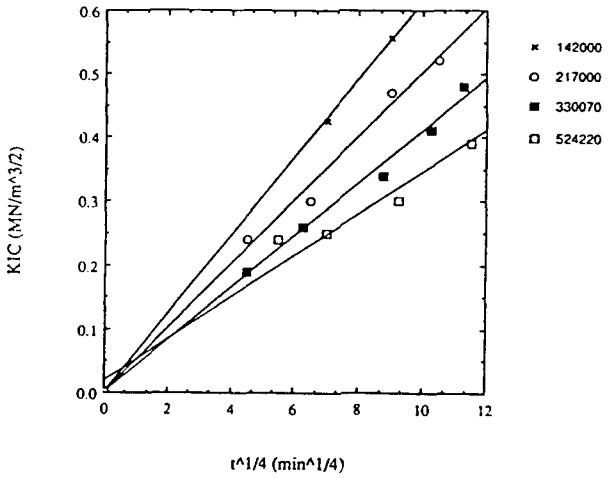

Fig. 19. K_{IC} vs. $t^{1/4}$ for welding of polystyrene of varying narrow fraction molecular weights using the wedge cleave technique (Wool and O'Connor).

Petrovska and Kausch (20) studied crack healing of PMMA using compact tension specimens with molecular weights of M_w = 88,500, 162,000, 404,000 and 727,000. The samples were fractured at room temperature and the recontacted surfaces were healed at 117°C. They found that their data could be described by Eq. 86 with x = 0.14. The effect of bond rupture in the healing experiments would be to lower the exponent for the molecular weight dependence, compared to welding of unfractured surfaces. In crack healing, the healing rate is determined by the effective molecular weight M_f, in the interface of thickness X. The number of broken bonds has been determined by Wool and Rockhill (17) as,

$$N_f = o\, N_x\, X/2\, (1/M_f - 1/M) \tag{87}$$

where N_f is the number of broken bonds per unit fracture surface area, N_a is Avogadro's number and M is the virgin state molecular weight. Appropriate values are $N_f = 5 \times 10^{13}/cm^2$ and X ≈ 1000 Å (or appropriate molecular weight dependence). Solving for Mf and substituting M_f for M in Eq. 86, it is easy to show that a lower exponent compared to the virgin state welding case would be obtained for the molecular weight dependence of the healing rate.

PMMA crack healing experiments of O'Connor (57) indicated that the time dependence of K_{Ic} was non linear on a $t^{1/4}$ scale which may be due to the molecular weight changes on the crack surfaces and the presence of craze fibrillar material. A higher

slope was observed at short healing times which changed to a lower slope at longer times. Higher molecular weight samples gave slower healing rates as observed by Kausch, et al. (20) but the data scatter in time and molecular weight did not permit a simple scaling law analysis using Eq. 86.

Fig. 20 shows G_{Ic} welding data at 115°C by McGarel and Wool (77, 78) for wedge cleavage welding of monodisperse molecular weight samples (152,000 and 400,000) of polystyrene. The data is plotted as G_{Ic} vs. $t^{1/2}M^{-1/2}$ (contour length). The data exhibits reasonable agreement with the contour length scaling law. Very little superposition was obtained when the data was plotted with respect to the bridge scaling law, $G_{1c} \alpha t^{1/2}M^{-3/2}$.

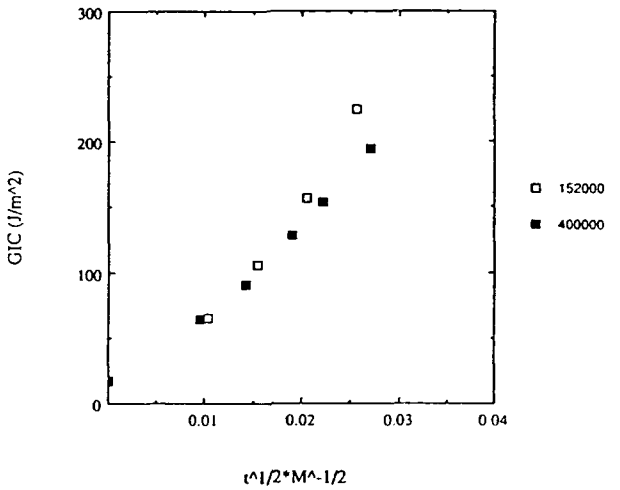

Fig. 20. G_{IC} vs. $t^{1/2}M^{-1/2}$ for welding of polystyrene of molecular weights 152,000 and 400,000 (Pressure Chemical) at 115°C (McGarel and Wool).

In accordance with the scaling laws for healing, if $G \alpha l(t)$ then the virgin state should support $G_{Ic\infty} \approx M$ for some range of molecular weight. Fig. 21 shows the fracture energy, G_{Ic}, of polystyrene as a function of molecular weight (monodisperse fractions) (50, 73, 77). An abrupt change in fracture behavior is observed in the vicinity of $M_c \approx 32{,}000$ which parallels changes in the zero-shear viscosity behavior. For $M < M_c$, the data obtained by Robertson (79) using wedge cleavage methods indicate that the material is very fragile with G_{1c} values of less than 1 J/m². The fracture energy in this region is well described by the linear equation,

$$G_{Ic} = 0.23 + 3.44x10\_5M \ (J/m^2). \qquad (88)$$

As M decreases, the fracture energy approaches the Griffith limit, $G_{Ic} = 2\Gamma$ where Γ is the surface energy. For PS at room temperature $2\Gamma = 0.08$ J/m² which is smaller than the extrapolated limit of 0.23 J/m² for the fracture energy in Fig. 21. However, this difference may be reasonable when consideration is given to the surface obtained by fracture compared with the flat surface normally used in surface tension measurements. The same data can also be described by a power law, $G_{Ic} = 4.67 \times 10^{-3}M^{0.53}$ J/m². It has been suggested by Kramer (80) from an analysis of the Robertson's data that $G_{Ic} \approx M^{1/2}$ based on the random-coil radius $\langle S^2 \rangle^{1/2} \approx M^{1/2}$ controlling the crack opening displacement at constant craze stress. The result, $G_{Ic} \approx M$, which is consistent with chain pullout arguments, provides a slightly better fit of the data in the molecular weight range $M < M_c$. The data are too limited and the function differences too small in the available data range to confidently determine the better approach.

In the molecular weight range $M_c < M < M^*$, where $M^* \approx 8M_c \approx 250{,}000$, G_{Ic} increases from 1 to 1000 J/m² as shown in Fig. 21 and can be described approximately by

$$G_{Ic} \approx (M^{1/2}-M_c^{1/2})^2. \quad (89)$$

The fracture data are normalized (by subtraction) to M_c. The physical meaning of this subtraction is that at M_c, the melt is critically entangled such that GIc ≈ 0 and an instability develops which does not require the removal of the average remaining bridge of length L_c. When $M \gg M_c$ but less than M^*, then the relation $G_{Ic} \approx M$ is realized. The uniaxial fracture stress, σ, and the critical stress intensity factor, K_{Ic}, both behave as $\sigma, K_{Ic} \approx (M^{1/2}-M_c^{1/2})$ in this range (1). Entanglement connectivity arguments based on percolation (84, 85) have been presented to explain the role of M_c in fracture of glassy polymers (4, 50). When $M > M_c$, chain pullout and disentanglement are dominant mechanisms of fracture in glassy polymers. The fracture surface morphology consists of fractured remnants of craze fibrillar material and considerable energy is expended in the formation and disentanglement of the craze microfibrils. The critical energy to propagate a crack through a craze zone is given by $G_{Ic} = \sigma_c\delta$ where σ_c is the stress necessary to form the craze and δ is the critical crack opening displacement. Both σ_c and δ should show a dependence on M and M_c which behaves approximately as $\sigma_c \approx \delta \approx (M^{1/2}-M_c^{1/2})$. Some support for this prediction is provided by fracture data on polycarbonate obtained by Pitman and Ward (81).

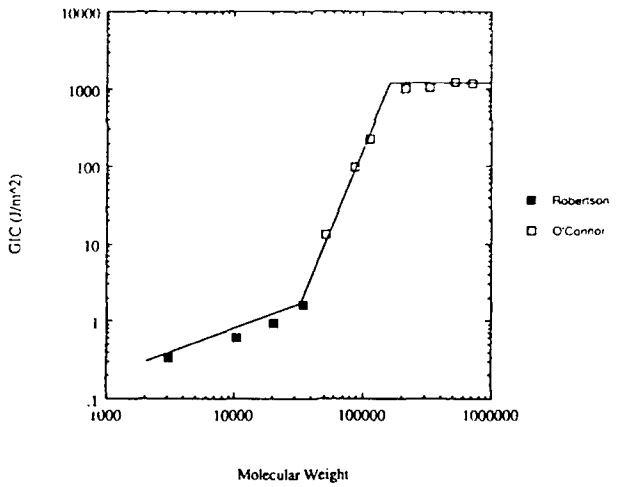

Fig. 21. G_{IC} vs. molecular weight for polystyrene in the virgin state. Data of Robertson (M < 40,000, filled points) and O'Connor and Wool (unfilled points).

When $M > M^*$, the fracture parameters become independent of molecular weight as shown in Fig. 21. The fracture energy attains an upper bound value of $G_{Ic} = 1000$ J/m². Upper bound values as low as 400 J/m² have also been reported and appear to depend on the notch preparation method. If the notch is exceedingly sharp, the lower value is obtained such that a single craze propagates ahead of the crack. Otherwise, craze bundles and other dissipative processes can contribute to the fracture energy. Welding of polymer interfaces provides an exceptionally sharp notch by virtue of the weak interface prepared with smooth surfaces. The asymptotic weld strength at $t \geq T_r$ converges on the true upper bound virgin state strength. Recent welding results of McGarel (78) suggest that the value of $G_{Ic} \approx 400$ J/m² is the correct upper bound "sharp" notch value for the virgin state fracture energy of PS. This observation leaves room for further interpretation of the molecular weight dependence of the fracture energy depicted in Fig. 21.

The number of broken bonds during fracture of PS in the upper bound molecular weight range was determined at room temperature as $N_f = 7 \times 10^{17}/m^2$ (17, 82, 83). Bond rupture contributes about 0.0001 kJ/m^2 to the fracture energy of 1 kJ/m^2 and is essentially negligible. However, the number of broken bonds roughly corresponds to the number of bridges crossing the fracture plane and suggests that bond rupture controls the extent of chain disentanglement and plastic deformation of the craze at $M > M^*$. Thus, in fracture of glassy polymers, viscous and plastic deformation processes dominate the energy consumption while bond fracture controls their extent. As the fracture temperature of PS is increased to T_g the number of broken bonds decreases (82, 83) and chain pullout is favored. Complete disentanglement ($N_f = 0$) is predicted to occur for PS at $T_g + 90°C$.

Prentice (42) and Evans (43) have argued that the fracture energy should depend on molecular weight via relations similar to Eq. 46 for chain pullout such that $G_{Ic} \approx n_\infty L^2$. While they incorrectly assume that $n_\infty \approx M^0$ (from Table 1, $n_\infty \approx M^{-1/2}$) they suggest that $G_{Ic} \approx L^2 \approx M^2$ and show from PMMA fracture data similar to that shown in Fig. 21 that a slope of 2 is obtained in the range $M_c < M < M^*$. A power law fit of the data in Fig. 21 indicates that $G_{Ic} \approx M^{3.4}$ but the slope of 3.4 is due to the inhomogeneous nature of G_{Ic} vs. M and the data is more justifiably represented by relations similar to Eq. 89 above. If the relation $G_{Ic} \approx M^2$ were correct, then one would expect the time dependence of welding as $G_{Ic}(t) \approx t/M$, but this is not consistent with welding data.

Effects of Pressure on Welding

The effect of the applied pressure on welding of monodisperse samples of polystyrene was studied by McGarel and Wool (97). Blocks of 52 x 52 x 3.5 mm of PS were welded at different pressures for 30 min at 115°C. The blocks were then cut into compact tension fracture mechanics specimens, the notch was fatigue sharpened at 10 Hz to produce a starter crack and the specimens were fractured at a rate of 0.25 mm/min at room temperature. When no pressure was applied during welding, the blocks pulled apart due to thermal contraction upon cooling. The effect of pressure on GIc at constant welding time is shown in Fig. 22. The fracture energy of the interface is seen to be independent of pressure above 0.4 MPa and G_{Ic} values were in the range of 327 to 385 J/m^2 which is below the virgin fracture value of 700 J/m^2.

The weld pressure influences the strength development in two ways. First, a certain amount of pressure is necessary to promote intimate contact and wetting of the polymer surfaces. Once good contact has been achieved the effect of pressures from 0.3-2.8 MPa (50 to 400 psi) appear negligible. At very high pressures, the glass transition temperature of PS increases by about 20°C per kilobar and this could have a substantial effect on welding rates at low weld temperatures.

Stacer and Schreuder-Stacer examined the effect of contact pressure on the autohesion of PIB (95). Fig. 23 shows their data for PIB surfaces contacted at progressively larger pressures. The data were obtained as described previously for Fig. 16 and the curves were shifted using the same WLF coefficients. Their data shows that as the pressure increases, G_a data appears to shift to shorter times and the welding time t_∞, decreases with no discernible effect on equilibrium G_∞ values. They suggest that the data support the contact mechanism for bond formation since the diffusion process would be independent of pressure in this pressure range.

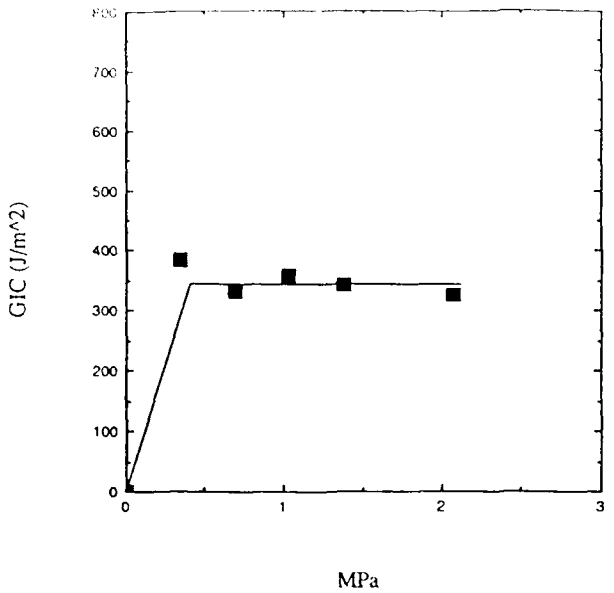

Fig. 22. G_{Ic} vs. contact pressure for welding of polystyrene at constant time of 30 min and temperature of 115°C. (McGarel and Wool).

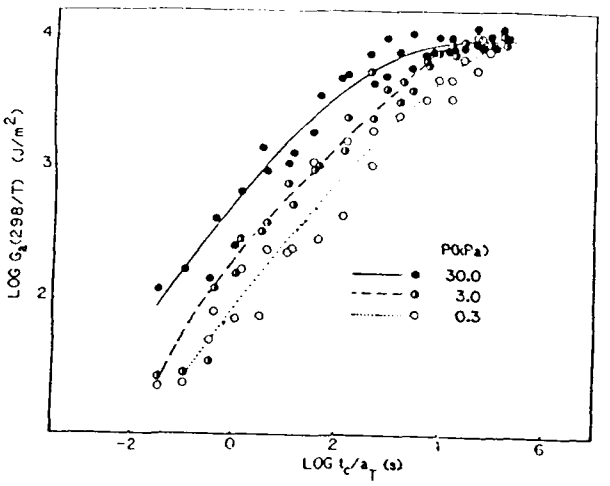

Fig. 23. Effect of contact contact pressure on the autohesion curve of PIB. (Stacer and Schreuder-Stacer).

Fatigue of Welded Interfaces

The effect of welding conditions on the fatigue crack propagation (FCP) rate, da/dN, along the welded PS/PS interface was investigated by Yuan and Wool (98). These experiments provide information on the expected lifetime of welded or laminated parts as a function of the time of welding. The basic question being addressed is to determine how the FCP rate of a partially healed interface compares with that of the fully healed state. Double cantilever beam (DCB) specimens as shown in Fig. 24, were machined from carefully welded plates of polystyrene. A thin Al-foil was placed in the interface at one end of the DCB to promote the initial crack start. Aluminum blocks with pin grips were glued to the DCB ends (Fig. 24). The fatigue tests were conducted in displacement δ, control mode with a haversine wave form at frequency 1 Hz and ratio $R = \delta_{min}/\delta_{max} = 0.33$.

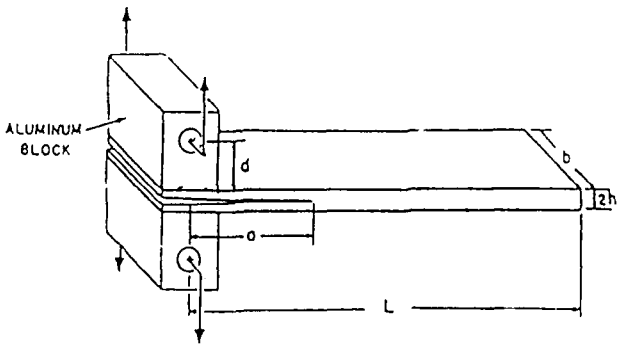

Fig. 24. DCB specimen for the fatigue testing of welded polystyrene plates with b = 12.7 mm, d = 12.7 mm and 2h = 6.6 mm. (Yuan and Wool).

The crack length a, was measured by a travelling microscope and the applied strain energy release value G_I, was calculated using the following expression by Wang (99),

$$G_I = 9(EI/a^4b)\,\delta^2[1 + 15/4\alpha(\delta/a) \qquad (90)$$

$$+ (189/64\,\alpha^2 + 6/7)(\delta/a)^2]$$

where E is the modulus, I is the moment of inertia and $\alpha = (d + h/2)/a$. The FCP rate is usually a power law in ΔG and can be described by

$$da/dN = A_{\Delta}G^m \tag{91}$$

where A and m are constants. In this experiment, the da/dN points were taken at the proper crack length to ensure applicability of beam theory and linear elastic fracture mechanics.

The FCP rate was determined at each welding time and was evaluated at a constant $G_I = 240\ J/m^2$. The results are shown in Fig. 25 for welding temperatures of 108°C and 117°C using PS samples with $M_n = 133{,}000$ and $M_w = 303{,}000$. A strong effect of welding time was noted and the results can be expressed as a power law,

$$(da/dN)_{\Delta G} = A(T)t^{-1.3} \tag{92}$$

where A(T) is a temperature dependent prefactor. Thus, as the strength of the interface increases with welding time, the FCP rate decreases with a strong power law dependence. The exponent of -1.3 compares with a theoretical value of -1.25 predicted using a chain disentanglement model (40, 50) such that

$$(da/dN)_{\Delta G} \alpha\ t^{-5/4}M^{5/4} \tag{93}$$

This relation suggests that at $t = T_r$, or when the virgin state is obtained that the molecular weight dependence of the FCP is determined by (50),

$$(da/dN)_{\Delta G} \alpha\ M^{-5/2} \tag{94}$$

Fig. 26 shows da/dN vs. molecular weight data of Hertzberg, et al. (100) and the strong molecular weight dependence is similar to that predicted by Eq. 94. It is interesting to note that when Berger and Kramer (51) examined the craze thickening velocity v_c, as a function of molecular weight, they found that $v_c \alpha M^{-5/2}$. The agreement between these results may be reasonable under stable crack-craze growth conditions.

The effects of a partially welded interface on the FCP rate are considerable as shown in Fig. 25. Many plastic parts are designed with regard to M^* such that G_{1c} (see Fig. 21) is a maximum at minimum melt viscosity. However, it is clear that enhanced fatigue lifetime can be obtained with $M > M^*$, as can be deduced from Fig. 26. These results are of importance for composite lamination of thermoplastic matrices. We propose further studies of fatigue-healing problems.

Fatigue crack healing is also an important concept for fiber filled composites. Klosterman and Wool (101) found that damage involving fiber-matrix failure and matrix cracking in glass fiber filled thermoplastics could be healed at temperatures above T_g. As a result, the FCP rate decreased with increasing healing time in the damage zone until the virgin state FCP rate was obtained. It was also found that complete crack healing could be obtained with highly cross-linked epoxies. These studies suggest that the lifetime of complex composites in practice could be considerably increased by periodic healing treatments. The possibility also exists that specific microwave and other treatments could be used to excite healing processes in specific regions of the composite.

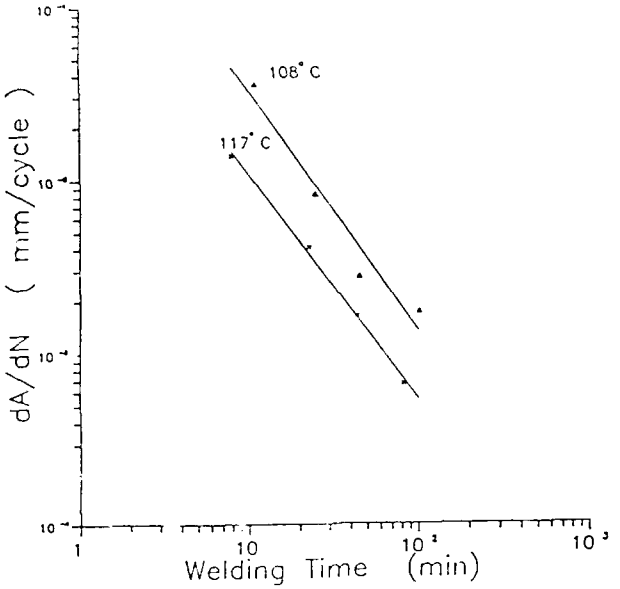

Fig. 25. Fatigue crack propagation rate of polystyrene vs. welding time at constant G = 240 J/m². M_n = 133,000 and M_w/M_n = 2.3. (Yuan and Wool).

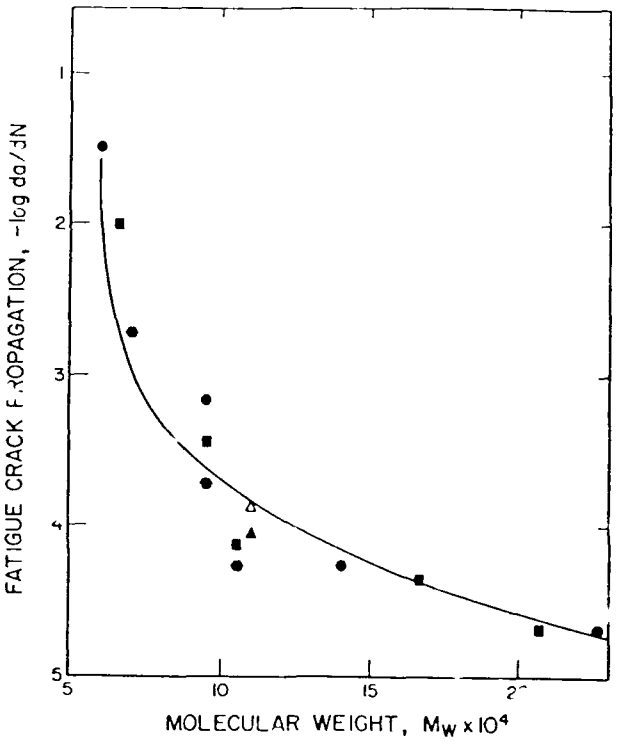

Fig. 26. Fatigue crack propagation rates vs molecular weight of PVC (Rimnac, et al.). The solid line is given by disentanglement theory by $da/dn = \alpha/(M^{5/2} - M_{cr}^{5/2})$ where $\alpha = 4.5 \times 10^{8}$ mm $M^{5/2}$ cycle and M_{cr} = 60,000 is the molecular weight at which critical crack propagation occurs at K = 0.7 MPa √m.

Incompatible Amorphous Interfaces

With immiscible, incompatible, amorphous polymers the equilibrium structure of the interface is determined thermodynamically by the balance of (1) the decrease of free energy due to entropy relaxation of the surface chain configurations and (2) the positive enthalpy of mixing produced by limited diffusion to a distance d_∞. Since $d_\infty \approx X^{-1/2}$ according to Helfand, et al. (24, 86) and the Flory-Huggins interaction parameter, X. behaves with temperature approximately as $X \approx 1/T$, we expect for fracture dominated by chain pullout that $G_{Ic} \approx l_\infty \approx d_\infty^2$ and that the equilibrium strength behaves with welding temperature as, (22, 77)

$$G_\infty \approx T. \tag{95}$$

The equilibrium fracture energy for several incompatible interfaces was obtained by Foster, Willett, et al. using wedge cleavage methods (77, 87, 102). These included PS/PMMA, PSAN/PMMA, PC/PSAN. G_{Ic} was found to increase with temperature in reasonable agreement with Eq. 95 for PSAN/PMMA and PC/PSAN interfaces but was fairly independent of temperature for PS/PMMA up to 170 C.. Typical measured fracture energies of order 40-200 J/m² were greater than either the initial wetted energy (about 5 J/m²) or the average surface energy, $\Gamma < 1.0$ J/m2, indicating that limited diffusion had taken place. The dynamics of welding incompatible, amorphous interfaces was found to be complex and will not be presented.

The equilibrium strength of incompatible interfaces occurs with full contact of the surfaces and appears to be dependent on the extent of the limited interdiffusion which is a function of temperature, molecular weight and chemical compatibility. For example, in Fig. 14, the SBR/Butyl interface in the autohesion experiment is incompatible and low strength is achieved compared to the symmetric SBR/SBR and Butyl/Butyl interfaces even though good contact has been achieved at very long times. This observation strongly supports the diffusion mechanism of strength development at amorphous polymer interfaces.

The magnitude of the equilibrium interpenetration distance, $d\infty$, can be approximated from the mechanical data using the following scaling relations,

$$[d_\infty/S_A]^2 = G_{Ic}(A/B)/G_{Ic}(A/A) \tag{96}$$

or,

$$[d_\infty/S_A] = \sigma(A/B)/\sigma(A/A) \tag{97}$$

where S_A is the radius of gyration of the pure A-component, $G_{Ic}(A/B)$ and $\sigma(A/B)$ are the equilibrium fracture properties of the incompatible pair and $G_{Ic}(A/A)$ and $\sigma(A/A)$ are the virgin state fracture properties of the A component. It is assumed that the pure polymers A and B have the same virgin state mechanical properties and molecular weights. For example, the butyl elastomer in Fig. 14 has a viscosity average molecular weight, M_v = 225,000 such that S ≈ 200 Å. If $\sigma(A/B)/\sigma(A/A) \approx 100/400$, then from Eq. 97, we obtain $d_\infty \approx 50$ Å.

For PS/PMMA interfaces, Foster and Wool (87), using wedge cleavage methods obtained constant values of GIc = 45 J/m² for welding at temperatures between 100 and 170°C. If we assume that for polystyrene with M = 250,000 and S = 138 Å that GIc(A/A) = 1000 J/m², as shown in Fig. 21, then from Eq. 96, $d\infty$ = 29 Å. The Flory-Huggins interaction parameter X, is related to $d\infty$ by $X = 0.66\,(b/d\infty)^2$, where b ≈ 6 Å is the statistical segment length. If $d\infty$ = 29 Å, then X ≈ 0.028 for the PS/PMMA interface. The temperature independence of the fracture energy for PS/PMMA interfaces are consistent with the very weak temperature dependence of X measured by Russell, et al. using neutron scattering techniques (103).

Incompatible Crystallizable Interfaces

Strength development at incompatible, crystallizable interfaces such as polyethylene with polypropylene, PE/PP, can occur by different mechanisms than those discussed above. In the melt, limited diffusion to a depth, d_∞, first occurs. When the interface cools, crystallization occurs first in the PP side due to the difference in melting points. Random nucleation of spherulites near the interface coupled with the volume contraction due to crystallization breaks up the interface. PE melt riverlets are drawn into the PP side which subsequently crystallize and effectively mechanically interlock the interface. This mechanism has been discussed by Galeski (88, 89) in terms of "local crystallization" creating "influxes" across the interface and has been investigated by Yuan and Wool (77, 90).

Fig. 27 shows a PE/PP interface during fracture by wedge cleavage methods. The interface was crystallized in a manner to optimize the mechanical interlocking effect. The fibrillar structures in the fractured interface are due to plastic deformation of the PE influxes. The fracture stress was measured as $\sigma \approx 10$ MPa which is more than half the virgin strength of PE. In the absence of influxes, the interface is extremely brittle with $\sigma <$

1 MPa. Fig. 28 shows a magnified view of the PP side obtained by SEM (90). The PE fibrillar remnants are clearly seen in the interstices of the PP spherulites. In addition to the influxes, PP spherulites which nucleate on the interface plane entrap PE melt on a finer scale between the crystalline lamellar structures as seen by the "white decoration" of plastically deformed PE on several PP spherulites.

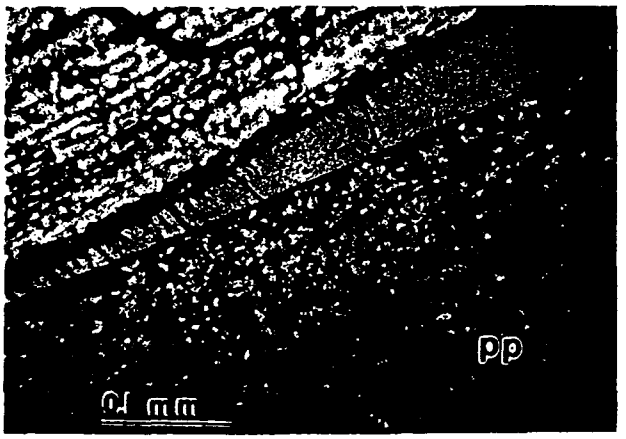

Fig. 27. Fracture of a PP/LLDPE incompatible semi-crystalline interface. The fibrils on the PE top surface are due to pullout of PE material which was incorporated into the PP side during crystallization (Yuan and Wool).

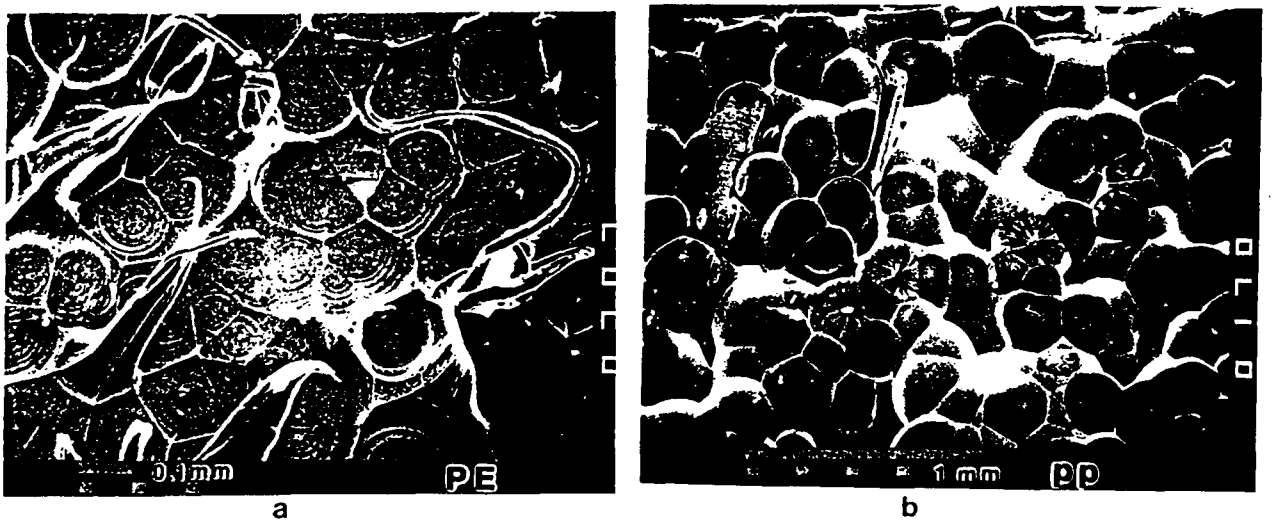

a b

Fig. 28. (a) Electron micrograph of a PE fracture surface from a PP/LDPE interface. Plastically deformed PE fibrils are observed in addition to circular imprints of PP spherulites on the PE side. (b) PP fracture surface from a PP/LDPE interface shows a fractured PE fibril remnant and PP spherulites (Yuan and Wool).

Thus, for incompatible, crystallizable interface, while melt diffusion produces an equilibrium interface of thickness 50 Å, the localized crystallization mechanism produces influxes to depths of several microns which impart significant strength to the interface. Delicate control of the processing history is necessary to optimize this effect as it is easy to make a weak interface with incompatible polymers. Methods of optimizing the strength have been discussed (90). The same mechanism also exists at the interface between symmetric crystallizable interfaces such as PE/PE welding but plays a secondary role to diffusion and homogeneous crystallization.

Lap Shear Welding

A lap shear method as shown in Fig. 29 was used to study strength development during welding of PS interfaces by Kline and Wool (91). The surfaces had previously not been in contact and care was taken to ensure rapid wetting of the interface. Lap shear samples were welded for a given time at constant temperatures above T_g and fractured at room temperature. Fig. 30 shows a plot of the (average of 15 samples) shear failure stress, τf, vs. time to the fourth power at each constant temperature. The linear response of τf with $t^{1/4}$ is seen at each temperature and provides further support for diffusion controlled strength at polymer-polymer interfaces.

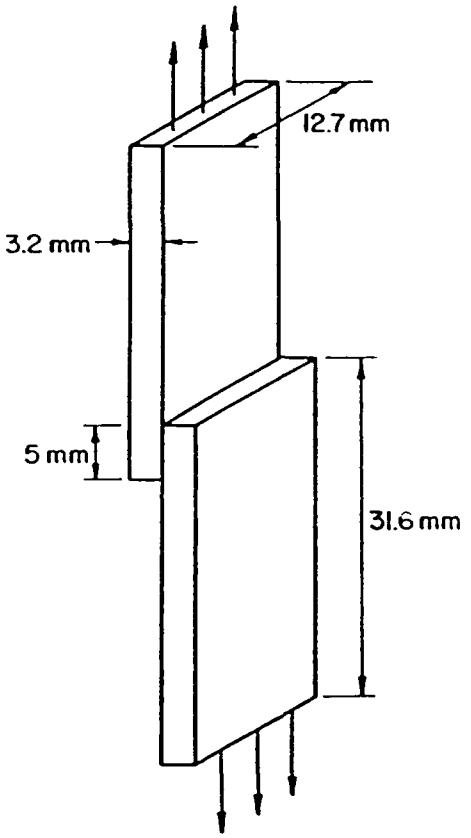

Fig. 29. Lap shear joint method used to test weld strength of polymers (Kline and Wool).

The change in slope with temperature was found to be describable by the William-Landel-Ferry (92) theory of thermal activation near T_g. At T = 113.5°C, the activation energy, E_a = 93.2 kcal/mole is predicted from a WLF analysis using the parameters for PS, c_1 = 13.7, c_2 = 50 and T_g = 100°C, which compares with E_a = 96.1 kcal/mole obtained from a plot of the superposition shift factor vs. 1/T in Fig. 30.

The time to achieve complete healing, T_h, can be estimated from the upper plateau in Fig. 30. At 391.3°K (118.1°C), $T_h \approx 256$ min for the polydisperse PS samples with M_n = 142,000 and M_w = 262,000. This time can be compared with related times measured by other techniques. Lee and Wool, (14) using FTIR dichroism techniques, measured the relaxation time, T_r, of uniaxially oriented monodisperse PS with M_n = 233,000 as T_r = 215 min. Kramer, et al. (93) report a self-diffusion coefficient for monodisperse PS with M_n = 255,000 as D = 5.8 x 10^{-17} cm²/sec at 125°C. Shifting to 118°C using the relation, (93)

$$\log D/T = A - B/(T-T_\infty), \qquad (98)$$

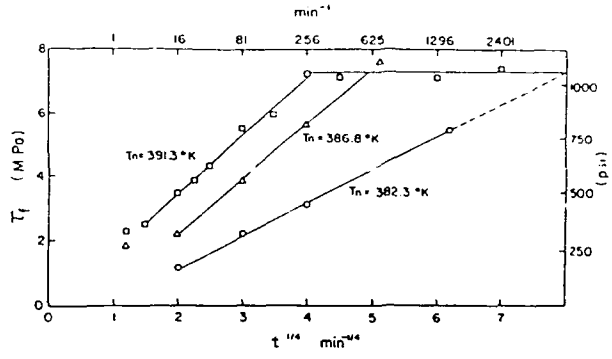

Fig. 30. Shear stress vs. $t^{1/4}$ for lap welding of polystyrene at several temperatures (Kline and Wool).

where B = 710, T_∞ = 49°C and A = -9.49, then $D_{118°C} = 6.42 \times 10^{-18}$ cm²/sec. Using Eq. 76, the time required for the center-of-mass to diffuse a distance equal to the end-to-end vector is obtained as T_r = 1000 min which is about 4 times longer than the time required to achieve complete strength of the lap shear joint with M_w = 262,000. On the other hand, using $T_r \approx$ M3 and D ≈ M-2, the relaxation time for the chains with Mn = 143,000 at 118°C is about 180 min which is in close agreement with the lap shear result. Because of the ramified nature of polymer interfaces with holes and statistical irregularities as shown in Fig. 7, the mechanical healing times are expected to be a little longer (but of the same order of magnitude) than the relaxation times determined from molecular dynamics and diffusion studies. It should be noted that when evaluating healing times from the reptation theory that at t = T_r, the center-of-mass of chains in the bulk diffuses a distance related to the end-to-end vector (Eq. 76), while the average monomer interpenetration distance at the polymer interface is equivalent to the radius of gyration (Eq. 17).

POLYMER PROCESSING WELD LINES

Compression Molding

As a final example of welding we consider the compression molding of resin pellets where the interfaces and weld lines form when the pellet surfaces contact in the mold as shown in Fig. 31. With increasing time and pressure, the interfaces wet, diffusion occurs and the strength of the sample increases to its virgin strength provided that sufficient time for diffusion is allowed.

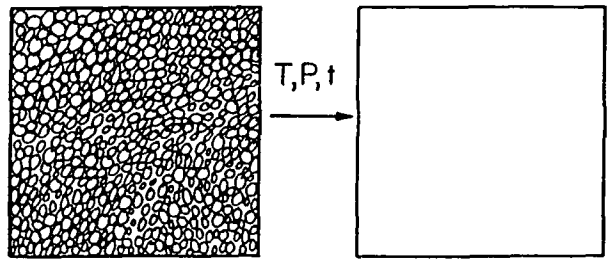

Fig. 31. Schematic of powder/pellet interface welding during polymer melt processing. With time, temperature and pressure, the pellet interfaces heal to form the plastic product.

Wool and O'Connor (1) studied the time-dependence of compression molding using PS pellets of the same molecular weight as described above in the lap shear experiments. PS plates, 152 by 152 mm, were compression molded in a Carver Press using a window frame 3.18 mm thick. Each plate was molded at 127°C± 6°C, with pressures of 5.5 MPa (800 psi) for varying processing times, t_p. The plate was withdrawn from the mold, quenched, cut into tensile "dogbone" samples and fractured at room temperature in uniaxial tension. Weak interfaces within the sample provided a source of crack initiation. Fig. 32 shows the

fracture stress (average of 6 samples) plotted vs. the fourth power of the processing time. The prediction of $\sigma(t) \approx t^{1/4}$ is again noted to be satisfactory despite the crudeness of the experiment. The processing time to reach the virgin state near $\sigma_\infty \approx 41.4$ MPa (6,000 psi) was between 10 and 20 min judging by the saturation of the strength at longer times. Using Kramer's diffusion data at 125°C, the reptation time for pellets with $M_n = 143{,}000$ is about 20 min which is in reasonable agreement with the observed processing time.

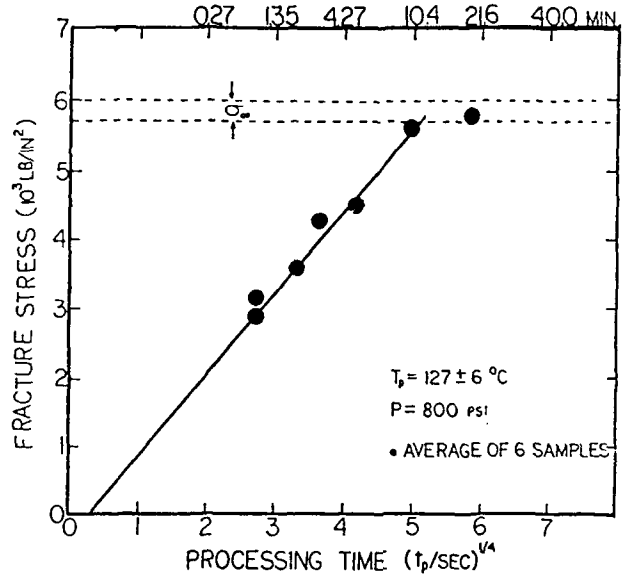

Fig. 32. Fracture stress vs. processing time ($t^{1/4}$) for compression molding of polystyrene pellets. Dogbone samples were prepared from compression molded plates (Wool and O'Connor).

The molecular weight dependence of the virgin strength, σ_∞, of compression molded PS pellets has been determined by McCormick, et al. (94) using similar sample preparation and fracture conditions. Fig. 33 (1) shows σ_∞ vs. $M^{1/2}$ for monodisperse molecular weight PS using data from reference 94. The data are described by

$$\sigma_\infty = 0.23(M^{1/2} - M_i^{1/2}) \text{ MPa}, \qquad (99)$$

where the intercept at $\sigma = 0$ is $\sqrt{M_i} = 245$. The strength is seen to increase linearly in accordance with virgin state predictions up to $M \approx 160{,}000$ after which it decreases slightly with increasing M. The data was obtained from samples compression molded at a constant time of 1 min at 170°C for all materials. We have suggested that under the processing conditions used that samples with $M < 160{,}000$ had reached their virgin state at $t = 1$ min but that samples with $M > 160{,}000$ were not completely healed at 1 min and the fracture stress should decrease as observed according to $\sigma \approx M^{-1/4}$. The reptation time for $M = 160{,}000$ is about 1 sec at 170°C and the time of 1 min used in this experiment presumably includes warm up time in the mold in addition to diffusion times. However, the maximum in strength with increasing M at constant contact time is expected and is similar to the tack and green strength data presented in Fig. 15.

Strength development at internal weldlines in injection molded specimens are expected to behave similarly although some complications are expected with interfaces involving oriented molecules at the weldline. However, it is interesting to note that orientation relaxation occurs at about the same rate as normal diffusion (14). Orientation relaxation may contribute to interdiffusion at the weldline in a similar manner as for unoriented surfaces but problems are anticipated with "barrier" effects produced by oriented layers which could result in anisotropic diffusion rates.

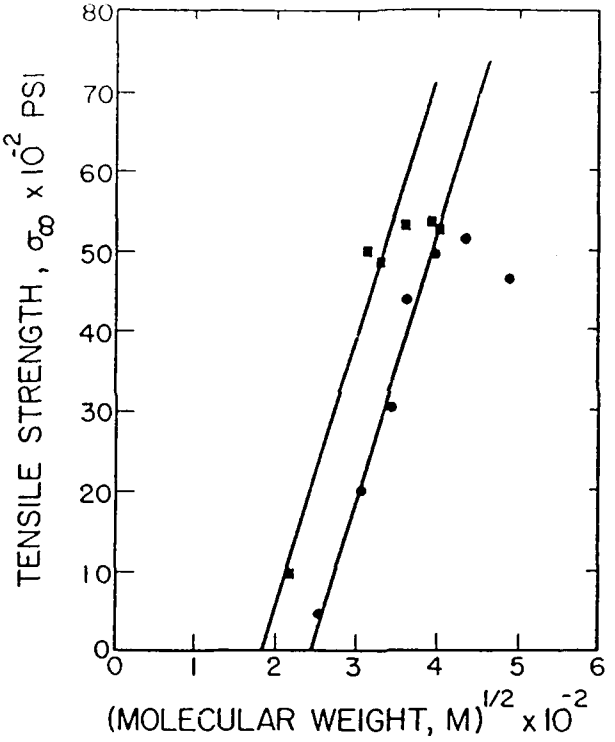

Fig. 33. Tensile strength vs. square root molecular weight of compression molded polystyrene (pellets). Molding occurred at 170°C for 1 minute. Monodisperse molecular weights pellets were used. Data of McCormick, et al.

Relation to Vibration Welding

Vibrational welds can be affected in thermoplastics over a frequency range 25-400 Hz, as reviewed by Stokes (104-107). Typical welding pressures are 130-2000 psi (1-14 MPa) with weld amplitudes of 0.3 to 1.6 mm. The welding process can be divided into four phases which are independent of the thermoplastic as follows. In Phase 1, the weld interface is heated by Coulombic friction which ends when the interface begins to melt. The penetration, which is the moving together of the separate pieces due to lateral flow out of the interface, is essentially zero during this phase. With continued energy input, the interface begins to melt and flow and penetration commences in Phase 2 up to a steady state lateral flow. Phase 3 represents the steady state flow condition during which the penetration increases linearly with time such that the material is melting at the same rate as it is flowing out of the lateral surfaces. The molten film is of the order of 0.1 to 0.23 mm and the temperature is very close to ambient within about 1.0 mm of the solid-liquid interface (105). Phase 4 occurs when the vibratory motion is stopped, and the interface solidifies.

The role of diffusion in vibrational welding is apparent in Phases 2-4. However, since the diffusion necessary to promote maximum strength involves distances of the order of 100 Å, the large amount of local melting (0.1 mm) and flow may be unnecessary. Obviously, the extent to which Phase 3 steady state flow is sustained determines the extent of lateral flow and local deformation of the weldline. For each thermoplastic, the temperature rise at the end of Phase 2 could be used to determine the healing time from the diffusion analysis and this could be used to minimize Phase 3 flow processes. For optimal component integrity, we would like to minimize contributions from Phases 2 and 3 by heating the interface in Phase 1 to cause melting and solidify in Phase 4. The pressure history could also be varied to promote melting in Phase 1 but with reduced pressure in Phases 2-4 to minimize flow. The reduced pressures used in vibrational welding would not affect the interdiffusion process once good contact had been achieved. The fact that flow occurs during Phase 3 at the interface presents new opportunities for mechanical interlocking and this could be important for incompatible interfaces.

CONCLUDING REMARKS

In this Report on welding mechanisms, we have examined strength development in terms of 1) the structure of the welded interface, 2) the microscopic deformation mechanisms and 3) the fracture mechanics of the weld. Attempts were made to relate the structure to strength using entanglement concepts and the dynamics of random-coil chains. The status of the description of the symmetric interface is such that we have significantly detailed information from the concentration profiles as shown in Table 1, provided the reptation model is the correct dynamics model. It is likely that more detailed models will evolve from current research. However, if one had to hypothesize at the nature of new models, it is most probable, based on the entanglement constraints to motion in polymer melts, that the framework of the reptation model would still be visible. The fractal nature of the diffusion front is generic to diffusion processes and provides useful physical insight into the structure and properties of interfaces.

The relation between structure and strength is complex and necessitates the use of new entanglement concepts in microscopic deformation models. The latter models and several simplifying assumptions used in this Report in relating structure to strength may be a cause of concern to the reader. This self-criticism points to the gap in our understanding of entanglement concepts and mechanical properties at the microscopic level. For example, the 3.4 exponent for the molecular weight dependence of the zero-shear viscosity remains an unsolved problem and impacts on our confidence to relate molecular dynamics to mechanical properties. It was the hope of this Report to present an analysis of strength development at polymer-polymer interfaces in a manner to indicate both their interesting complexity and suggest pathways for solutions to interface problems.

ACKNOWLEDGEMENTS

The author is grateful for the financial support of the Army Research Office, Durham, NC, Grant DAAL03-86-K-0034. The students funded by this contract were Owen McGarel, Baoling Yuan and Ken Foster.

REFERENCES

1. R. P. Wool and K. M. O'Connor J. Appl. Phys. 52 (10), 5953-5963 (1981).
2. Y.H. Kim and R. P. Wool Macromolecules 16, 1115-1120 (1983).
3. R. P. Wool Rubber Chem. Technol. 57 (2), 307-318 (1984).
4. R. P. Wool J. Elastomers and Plastics 17 (April), 107-118 (1985).
5. P.-G. de Gennes J. Chem. Phys. 55, 572-579 (1971).
6. S. F. Edwards Proc. Phys. Soc., London 92, 9 (1967).
7. S. Prager and M. Tirrell J. Chem Phys. 75 (10), 5194-5198 (1981).
8. K. Jud, J. G. Williams, and H. H. Kausch J. Mater. Sci. 16, 204 (1981); H. H. Kausch Pure Appl. Chem. 55, 833 (1983).
9. P.-G. de Gennes C. R. Acad. Sci., Paris 292 (2), 1505 (1981).
10. S. Wu Polymer Interfaces and Adhesion; Dekker: New York, 1982.
11. S. Voyutskii "Autoadhesion and Adhesion of Polymers," Polymer Revs. 4, H. F. Mark and E. H. Immergut, Eds.; Wiley Interscience: New York, 1963.
12. M. Doi and S. F. Edwards Faraday Trans. 2, 1789 (1978).
13. M. Tirrell Rubber Chem. Technol. 57 (3), 523-556 (1984).
14. (a) A. Lee and R. P. Wool Macromolecules 19, 1063-1068, (1986); Macromolecules 20, 1924 (1987). (b) W. Walczak and R. P. Wool, Bull. Amer Phys. Soc. 34, 854 (1989).
15. H. Zhang and R. P. Wool Macromolecules 22, 000 (1989).
16. R. P. Wool Proc. IX Intl. Congress on Rheology 3, 573-580, Acapulco, Mexico (1984).
17. R. P. Wool and A. T. Rockhill J. Macromol. Sci.-Phys. B20 (1), 85-99 (1981).
18. H. H. Kausch Polymer Fracture, 2nd Ed., Ch. 10; Springer: Heidel berg, 1987.
19. K. Jud and H. H. Kausch Polym. Bull. 1, 697 (1979); H. H. Kausch and K. Jud Plastics & Rubber Proc. & Appl. 2, 265 (1982).
20. D. Petrovska-Delacretaz and H. H. Kausch, Proceedings of IBM Polymer Symposium, Florence Italy May 10 (1989).
21. R. P. Wool and K. M. O'Connor J. Polym Sci., Polym Lett. Ed. 20, 7 (1982).
22. J. L. Willett, K. M. O'Connor, and R. P. Wool ACS Polym. Pre-pr. 26 (2), 123-125 (1985).
23. S. J. Whitlow and R. P. Wool Macromolecules 22, 000 (1989); R. P. Wool, Bull. Amer. Phys. Soc. 32, (1987).
24. E. Helfand and Y. Tagami J. Chem. Phys. 56, 3592 (1972).
25. P. J. Flory Principles of Polymer Chemistry; Cornell University Press: Ithaca, NY, 1953.
26. P.-G. de Gennes C. R. Acad. Sci., Ser. B 291 (Nov), 219-221, (1980).
27. P. G. de Gennes and L. Leger Ann. Rev. Phys. Chem. 33, 49-61 (1982).
28. (a) D. Adolf, M. Tirrell, and S. Prager J. Polym. Sci., Polym. Phys. Ed. 23, 413-427 (1985). (b) M. Tirrell, D. Adolf, and S. Prager IMA Vols. in Math and Its Applications 5, Springer-Verlag (1986).
29. A. G. Mikos and N. A. Pappas J. Chem. Phys. 88 (2), 1337 (1988).
30. B. Sapoval, M. Rosso, and J. F. Gouyet J. Physique, Lett. (Paris) 46, 149-156 (1985).
31. M. Rosso, J. F. Gouyet, and B. Sapoval Phys. Rev. Lett. 57 (25),

3195-3198 (1986).
32. M. Kolb, J. F. Gouyet, and B. Sapoval Europhys. Lett. 3 (1), 33-38 (1987).
33. B. B. Mandelbrot The Fractal Geometry Of Nature; Freeman and Co.: San Francisco, 1982.
34. R. P. Wool and J. M. Long Proc. US-Germany Polymer Science Sympo sium, Napa Valley, CA, Sept. 1987; R. P. Wool and J. M. Long, in press, (1990).
35. S. Mazur and S. Reich J. Phys. Chem. 90, 1365-1372 (1986).
36. R. P. Wool, "Dynamics and Fractal Structure Of Polymer Interfac es", Chapter in New Trends in Physics and Physical Chemistry, L.-H. Lee, Ed., Plenum Press, New York (1989).
37. A. A. Griffith Phil. Trans. Roy. Soc. A221, 163 (1920).
38. R. E. Robertson "Toughness and Brittleness in Plastics," Adv. in Chem., No. 154; American Chemical Society: Washington, D.C., 1976, p. 89.
39. E. J. Kramer J. Mater. Sci. 14, 1381-1388 (1978).
40. R. P. Wool ACS Polym. Preprints 23 (2), 62 (1982).
41. R. P. Wool, Invited Lecture, Bull. APS 27, 297 (1982).
42. P. Prentice Polymer 24, 344-350 (1983).
43. K. E. Evans J. Polym. Sci., Polym. Phys. Ed. 25, 353-368 (1987).
44. D. S. Dugdale J. Mech. Phys. Solids 8, 100-104 (1960).
45. J. R. Rice, in Fracture 2 (3), H. Liebowitz, Ed.; Academic Press, 1968.
46. L. C. Dolmon, I. M. Robertson, and R. P. Wool Bull. APS 30 (3), 488 (1985).
47. B. D. Lauterwasser and E. J. Kramer Phil. Mag. A 39 (4) 469-495 (1979).
48. E. Paredes and E. W. Fischer J. Polym. Sci., Phys. Ed. 20, 929 (1982).
49. A. M. Donald and E. J. Kramer J. Polym. Sci., Polym. Phys. Ed. 20, 899-909 (1982).
50. R. P. Wool in "Amorphous Polymers and Non-Newtonian Fluids," IMA Vols. in Math 6, 169-187, C. Dafermos, J. L. Ericksen, and D. Kinderlehrer, Eds.; Springer-Verlag, 1987.
51. L. L. Berger and E. J. Kramer Macromolecules, 20, 1980 (1987).
52. H. H. Kausch, Lecture presented to Mater. Res. Soc., Boston, Dec. 1987.
53. R. P. Wool and K. M. O'Connor Polym. Eng. and Sci. 21, 970-977 (1981).
54. (a) O. J. McGarel and R. P. Wool J. Polym. Sci., Phys. Ed. 25, 2541 (1987); (b) Bull. Amer. Phys. Soc., 34(3) 939 (1989).
55. K. M. O'Connor and R. P. Wool J. Appl. Phys. 51, 5075-5079 (1980).
56. R. P. Wool, in Adhesion and Adsorption of Polymers, Part A, 341-362, L.-H. Lee, Ed.; Plenum Press: New York, 1980.
57. K. M. O'Connor "Crack Healing in Polymers," PhD Thesis Disserta tion, University of Illinois, 1984.
58. G. R. Hamed Rubber Chem. Technol. 54, 576-595 (1981).
59. C. K. Rhee and J. C. Andries Rubber Chem. Technol. 54, 101-114 (1981).
60. R.-J. Chang and A. N. Gent J. Polym. Sci., Phys. Ed. 19, 1619-1633 (1981).
61. J. D. Skewis Rubber Chem. Technol. 39, 217 (1966).
62. W. G. Forbes and L. A. McLeod Trans. I.R.I. 30 (5), 154-174

(1958).
63. J. D. Skewis private communication, and Reference 61.
64. G. R. Hamed and C.-H. Shieh J. Polym. Sci., Polym. Phys. Ed. 21, 1415 (1983).
65. T. Tsuji, M. Masuoko, and K. Nakao in Reference 71.
66. A. K. Bhowmick, P. P. De, and A. K. Bhattacharyya Polym. Eng. and Sci., in press (1987).
67. E. Bister, W. Borchand, and G. Rehage Kaut. und Gummi Kunst. 29, 527 (1976).
68. S. Wu, K. K. Chuang, and C. D. Han J. Polym. Sci., Phys. Ed. 24, 143-156 (1986).
69. C. M. Roland and G. G. A. Bohm Macromolecules 18, 1310-1314 (1985).
70. R. M. Vasenin Adhes. Age 8 (5), 18 (1965).
71. L.-H. Lee, Ed., Adhesion and Adsorption of Polymers, 12A and 12B, Plenum Press: New York (1980).
72. J. N. Anand Adhesion 1, 31 (1969).
73. K. M. O'Connor and R. P. Wool Bull. APS 30 (3), 389 (1985).
74. R. P. Wool, Final Report, "Crack Healing In Polymers", U.S. Army Research Office Grant DAAG-29-C-0143, Durham, NC (1983); "Weld ing, Tack and Green Strength of Polymers", Chapter in Fundamen tals of Adhesion, Ed. L.-H. Lee; Plenum Press: New York, 1989.
75. R. Guernsey and J. Gilman Exptl. Mech. 1, 50 (1961).
76. M. F. Kanninen Intl. J. Fracture 9, 83 (1973).
77. R. P. Wool, J. L. Willett, O. J. McGarel, and B.-L. Yuan ACS Polym. Prepr. 28 (2), 38 (1987).
78. O. J. McGarel, Ph. D. Thesis work in progress.
79. R. Robertson used the Wedge Cleavage method in Reference 38.
80. E. J. Kramer derived GIc = $\sigma c(\alpha\text{-}1)R^2$ ~M1/2 in Reference 39.
81. G. L. Pitman and I. M. Ward Polymer 20, 897-902 (1970).
82. J. L. Willett, K. M. O'Connor, and R. P. Wool J. Polym. Sci., Polym. Phys. Ed. 24, 2583-2589 (1986).
83. K. Paulson and R. P. Wool, to be published.
84. S. Feng and P. N. Sen Phys. Rev. Lett. 52 (3), 216-219 (1984).
85. H. He and M. F. Thorpe Phys. Rev. Lett. 54 (19), 2107-2109 (1985).
86. (a) E. Helfand, in Polymer Compatibility and Incompatibility, M. Solc, Ed.; MMI Press: Midland, MI, 1983. (b) T. A. Weber and E. Helfand Macromolecules 9, 311 (1976).
87. K. L. Foster and R. P. Wool Macromolecules, in press.
88. Z. Bartzak and A. Galeski Polymer 27, 544-548 (1986).
89. A. Galeski and E. Piorkowska J. Polym. Sci., Polym. Phys. Ed. 21, 1299 (1983).
90. B.-L. Yuan and R. P. Wool, Polym. Eng. and Sci., in press (1990).
91. D. B. Kline and R. P. Wool, Polym. Eng. and Sci. 28, 52 (1988).
92. J. D. Ferry, Viscoelastic Properties of Polymers, 3rd Ed.; Wiley: New York, 1980.
93. P. F. Green and E. J. Kramer Macromolecules 19, 1108 (1986); E. J. Kramer, private communication.
94. H. W. McCormick, F. M. Brower, and L. Kin J. Polym. Sci. 39, 87 (1959).
95. R. G. Stacer and H. L. Schreuder-Stacer Intl. J. Fracture 39, 201 (1989).
96. N. S. Korenevskaya, V. V. Laurent'ev, S. M. Yagnyatinskaya, V. G. Rayevskii and S. S. Voyutskii Polymer Science USSR 8, 1372

(1966).
97. O. J. McGarel and R. P. Wool Bull. Am. Phys. Soc. March, 1989.
98. B. Yuan and R. P. Wool Bull. Am. Phys. Soc. March, 1989.
99. S. S. Wang J. Composite Mater. 20, 439 (1986).
100. C. M. Rimnac, J. A. Manson, R. W. Hertzberg, S. M. Webler and M. D. Skibo Macromol. Sci-Phys. B19, 351 (1981).
101. D. H. Klosterman and R. P. Wool Bull. Am. Phys. Soc. March, 1982.
102. J. L. Willett "Strength Development at Incompatible Polymer In terfaces," PhD Thesis, University of Illinois, 1988.
103. T. Russell Macromolecules, in press; private communication.
104. V. K. Stokes, Polym. Eng. Sci. 28, 718 (1988).
105. V. K. Stokes, Polym. Eng. Sci. 28, 728 (1988).
106. V. K. Stokes, Polym. Eng. Sci. 28, 989 (1988).
107. V. K. Stokes, Polym. Eng. Sci. 28, 998 (1988).